FINAL REPORT: CHANNEL CHARACTERIZATION FOR FREE-SPACE OPTICAL COMMUNICATIONS
Phase 0 Testing at Hollister, CA
Phase 2 Final Testing at China Lake, CA

UCF DARPA Project ID: 66016010

July 2012

L. C. Andrews, R. L. Phillips
Consultants for UCF

R. Crabbs, T. Leclerc, and P. Sauer
Florida Space Institute (FSI), University of Central Florida,
MS: FSI, Kennedy Space Center, FL 32899

This work was funded by the Defense Advanced Research Projects Agency (DARPA) in support of the ORCA/FOENEX Project with Program Manager Dr. Larry Stotts, and subsequently Dr. Richard Ridgway. Distribution Statement "A" (Approved for Public Release, Distribution Unlimited).

Report Documentation Page

Form Approved
OMB No. 0704-0188

1. REPORT DATE	2. REPORT TYPE	3. DATES COVERED
JUL 2012		**00-00-2012 to 00-00-2012**

4. TITLE AND SUBTITLE	5a. CONTRACT NUMBER
Channel Characterization For Free-Space Optical Communications	5b. GRANT NUMBER
	5c. PROGRAM ELEMENT NUMBER
6. AUTHOR(S)	5d. PROJECT NUMBER
	5e. TASK NUMBER
	5f. WORK UNIT NUMBER
7. PERFORMING ORGANIZATION NAME(S) AND ADDRESS(ES) **University of Central Florida,Florida Space Institute (FSI),MS: FSI,Kennedy Space Center,FL,32899**	8. PERFORMING ORGANIZATION REPORT NUMBER
9. SPONSORING/MONITORING AGENCY NAME(S) AND ADDRESS(ES)	10. SPONSOR/MONITOR'S ACRONYM(S)
	11. SPONSOR/MONITOR'S REPORT NUMBER(S)

12. DISTRIBUTION/AVAILABILITY STATEMENT
Approved for public release; distribution unlimited

13. SUPPLEMENTARY NOTES

14. ABSTRACT

15. SUBJECT TERMS

16. SECURITY CLASSIFICATION OF:			17. LIMITATION OF ABSTRACT	18. NUMBER OF PAGES	19a. NAME OF RESPONSIBLE PERSON
a. REPORT **unclassified**	b. ABSTRACT **unclassified**	c. THIS PAGE **unclassified**	**Same as Report (SAR)**	**60**	

SUMMARY

The current DARPA Free space Optical Experimental Network Experiment (FOENEX) Program is a continuation of the earlier Optical RF Communications Adjunct (ORCA) Program that was designed to bring high data rate networking to the warfighter via airborne platforms. The FOENEX program is headed by the Applied Physics Laboratory (APL) of the Johns Hopkins University. Radio frequency (RF) equipment and networking was designed and built by L3 and the adaptive optics (AO) subsystem was designed and built by AOptix. Phase 0 testing of the FOENEX hybrid system took place during June 2011 at Hollister Air Force Range in California and Phase 2 Final Testing was performed in March and April of 2012 at the Naval Air Weapons Test Range in China Lake, California. The University of Central Florida (UCF) was separately contracted by DARPA to measure path-averaged values of the refractive-index structure parameter C_n^2, the inner scale of turbulence l_0, and the outer scale of turbulence L_0 along the propagation path from a Twin Otter aircraft to a ground site (G6) at China Lake, CA. The nominal range to the aircraft from the ground site at G6 was 50 km, but variations in range extended from 30 km to 75 km. Although not part of the original Statement of Work (SoW), UCF also provided the same measurements at Hollister Air Force Range between the Hollister Airport and Fremont Peak over a path length of 17 km. In addition, UCF researchers also provided a comparison of theoretical models with measured quantities from the optical data beam during testing at both sites to ascertain some assessment of system performance.

The UCF team took direct measurements of only the beacon beam at Hollister and China Lake which led to path-averaged values for the atmospheric parameters. From the path-average parameters, a C_n^2 profile model, called the HAP model, was constructed so that the entire channel from air to ground, ground to air, and from air to air can be characterized. This HAP model permits an accurate estimation of the Fried parameter r_0 and the Strehl Ratio (SR), both of which are required to estimate the Power in the Bucket (PIB) and Power in the Fiber (PIF) associated with the FOENEX data beam. UCF was provided with some of the PIB and PIF data taken by APL on the FOENEX data beam in order to compare actual measurements with theoretical predictions based on the HAP model.

During measurements at Hollister Airport, the path-average C_n^2 data were fairly consistent from day to day without regard to time of day. For example, on June 7 the overall C_n^2 average was 2.22×10^{-15} $m^{-2/3}$, on June 8 the overall average was 2.29×10^{-15} $m^{-2/3}$ (1:00-2:00 pm) and 1.94×10^{-15} $m^{-2/3}$ (5:10-6:15 pm), and on June 9 the overall average was 2.08×10^{-15} $m^{-2/3}$. Using these overall averages of the path-average values of C_n^2, the resulting HAP C_n^2 profile model led to values of ground level C_n^2 that compared very well with actual measurements of the BLS-900 Scintec scintollometer controlled by APL. The same was true of the theoretical and measured PIB in both directions over the 17-km range during the Phase 0 testing at Hollister. However, in only one case (June 7, 2011, 6:30 pm) did the theoretical estimates of PIF compare well with actual measurements of

PIF. In cases where disagreement between theoretical and actual measurements of PIF data existed, the PIF theoretical values with AO turned on were generally higher than measured PIF data by as much as 6-15 dB. The only explanation for this disagreement is that the AO subsystem could not always get the captured PIB light into the single-mode optical fiber, possibly because of changing atmospheric effects that caused a mode mismatch that the AO system could not correct. The Fried parameter r_0 was derived from the HAP model and found to vary from around 2 cm to nearly 6 cm at the Fremont end of the Hollister link. These variations are caused by changing ground-level conditions during different times of the day. At the Hollister Airport end of the link the Fried parameter was a little smaller, varying from 1.5 cm up to around 4 cm. These estimates of the Fried parameter were used in calculating the theoretical estimates of PIB and PIF at both ends of the link.

During Phase 2 testing at China Lake the atmospheric parameters showed a lot of fluctuations compared with that at Hollister. UCF collected path-average data on March 19-21, 2012 and on April 2-3, 2012. Path-average C_n^2 values on March 20 were averaged over 1-hr periods and showed variations between 0.6×10^{-16} and 1.24×10^{-16} $m^{-2/3}$. On April 2 and 3 the mean path-average values were 2.23×10^{-16} and 3.6×10^{-16} $m^{-2/3}$, respectively. Because of FOENEX system problems during the testing period, only the PIB and PIF data taken on April 2 and 3, 2012 were analyzed. The HAP model led to ground level C_n^2 values on the order of 10^{-13} to 10^{-12} $m^{-2/3}$, consistent with those measured with the UCF SLS-20 Scintec scintillometer on April 2 and 3. Using the HAP C_n^2 profile model, the average downlink Fried parameter at China Lake varied from 4.9 cm on April 2 to 2.4 cm on April 3. The average uplink Fried parameter ranged from 21.3 cm on April 2 to16.3 cm on April 3. Theoretical estimates of PIB were 0.0 dBm (downlink) and –1.7 dBm (uplink) on April 2, and –0.9 dBm (downlink) and –4.0 dBm (uplink) on April 3. Theoretical estimates of PIF ranged from –7.7 dBm (downlink) to –9.7 dBm (uplink) on April 2, and –10.4 dBm (downlink) to –12.2 dBm (uplink) on April 3. For the air-to-air path on April 3 at China Lake the theoretical average mean PIB was around 1.9 dBm at 40 km range and -17.5 dBm at 160 km. Similarly, the theoretical mean PIF was –4.9 dBm at 40 km and –24.3 dBm at 160 km. Air-to-air data was not useful from April 2 and that on April 3 was not as definitive as air-ground data, partially because of the large variations in range from 40 km to 160 km. The Fried parameter in the air-to-air link was always larger than the receiver aperture.

As a final comment, we note that although the theoretical mean PIB was always in good agreement with the measured PIB, this was not always the case with the mean PIF. In fact some of the theoretical results with no receiver (Rx) AO provided a better fit with the measured data than the theoretical result with full Rx AO compensation. It is believed that this happened when the atmospheric-caused scintillation was sometimes too strong for the AO system to focus the captured light into the single-mode fiber due to amplitude mode mismatch.

TABLE OF CONTENTS

1. INTRODUCTION

The current DARPA Free space Optical Experimental Network Experiment (FOENEX) Program is a continuation of the earlier Optical RF Communications Adjunct (ORCA) Program that was designed to bring high data rate networking to the warfighter via airborne platforms. Phase I testing of the ORCA system from/to an aircraft to/from a mountaintop was conducted in May 2009 by the Northrop Grumman Corporation (NGC) at the Nevada Test and Training Range (NTTR) located on the Nellis Air Force Range near Tonopah, Nevada. The follow-on FOENEX program is now headed by the Applied Physics Laboratory (APL) of the Johns Hopkins University and preliminary Phase 0 testing was conducted in June 2011 at the Hollister Air Force Range in California and Phase 2 Final Testing was performed during March-April, 2012 at the Naval Air Weapons Test Range in China Lake, California.

The University of Central Florida (UCF) was separately contracted by DARPA for both the ORCA and FOENEX programs to measure weighted path-averaged values of the refractive-index structure parameter C_n^2, the inner scale of turbulence l_0, and the outer scale of turbulence L_0 along the propagation path. This was accomplished using the three aperture scintillometer system (TASS) developed by the Wave Propagation Research Group (WPRG) at the Townes Laser Institute of UCF. The TASS measures the scintillation of the FOENEX beacon beam in three different sized apertures. From a mathematical model of the scintillation as measured with three apertures the inverse problem is solved for the parameters that created the scintillation. This report presents background information on measured atmospheric conditions for Phase 0 testing at the Hollister site and Phase 2 testing at China Lake, mathematical models that were used for the analysis, and a C_n^2 profile model as a function of altitude that was deduced from the path-averaged parameters. Based on the UCF measurements, an estimation of ground level C_n^2 values were calculated and compared with those of a commercial Scintec BLS 900 scintillometer at Hollister and SLS-20 scintillometer at China Lake. Further estimation of the average data beam Power in the Bucket (PIB) and Power in the Fiber (PIF) during testing was done by UCF and compared with actual measurements of the data beam PIB and PIF during testing. All UCF estimates of PIB and PIF were based on average values of the path-average atmospheric parameters rather than point by point.

2. SUMMARY OF SOW TO DARPA

From the Statement of Work (SOW) dated July 9, 2010, the following tasks were proposed.

Tasks

The instrumentation for the channel will be designed, built and tested on instrumented ranges at the Space and Naval Warfare Center's, Innovative Science and Technology Facility at Kennedy Space Center. The tasks to be performed are: (1) Theoretical

Modeling, (2) Receiver Design and Construction, (3) Testing on Instrumented Range, (4) Deploying and Field Operations and (5) Data Processing, (6) Reporting

The Deliverables to DARPA listed in the SOW are given below.

Deliverables

a) Monthly status reports
b) Data analysis during testing, as close to real time as possible
c) Final report and analyses

Although the SOW for UCF included only the Final Testing to be done at China Lake, the UCF team sent two researchers to Hollister Air Force Station in California to conduct path-average measurements that could characterize the atmospheric conditions over the 17-km range during Phase 0 testing. In this report, we present the results of those measurements along with those from the Final Testing at China Lake.

3. ATMOSPHERIC CHARACTERIZATION

Atmospheric turbulence is often characterized by a single parameter C_n^2 (in units of $m^{-2/3}$), called the refractive index structure parameter. However, in scintillation studies it is also useful to have knowledge of the refractive-index inner scale l_0 and outer scale of turbulence L_0. Both C_n^2 and the inner scale impact the scintillation index under weak irradiance fluctuations, whereas all three parameters play a role in the behavior of the scintillation index in regimes of moderate-to-strong irradiance fluctuations (see Fig. 1).

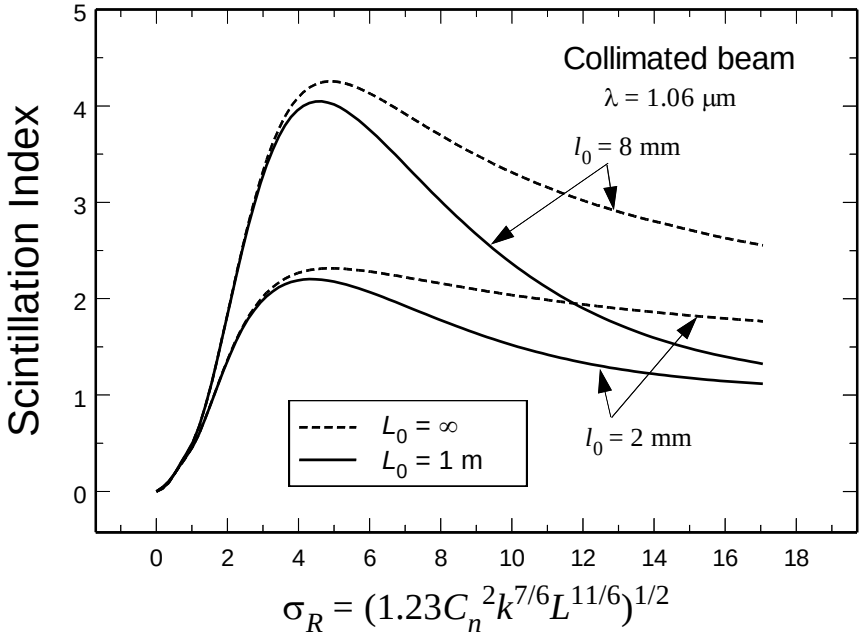

Figure 1 Scintillation index as a function the square-root of Rytov variance showing the influence of both inner and outer scales.

In addition to the influence of inner and outer scale, scintillation also varies with receiver (Rx) aperture size. That is, as the Rx aperture grows larger, the scintillation is reduced—an effect widely known as aperture averaging. We illustrate this idea in Fig. 2 where we plot the scintillation index for various values of inner scale as a function of aperture diameter.

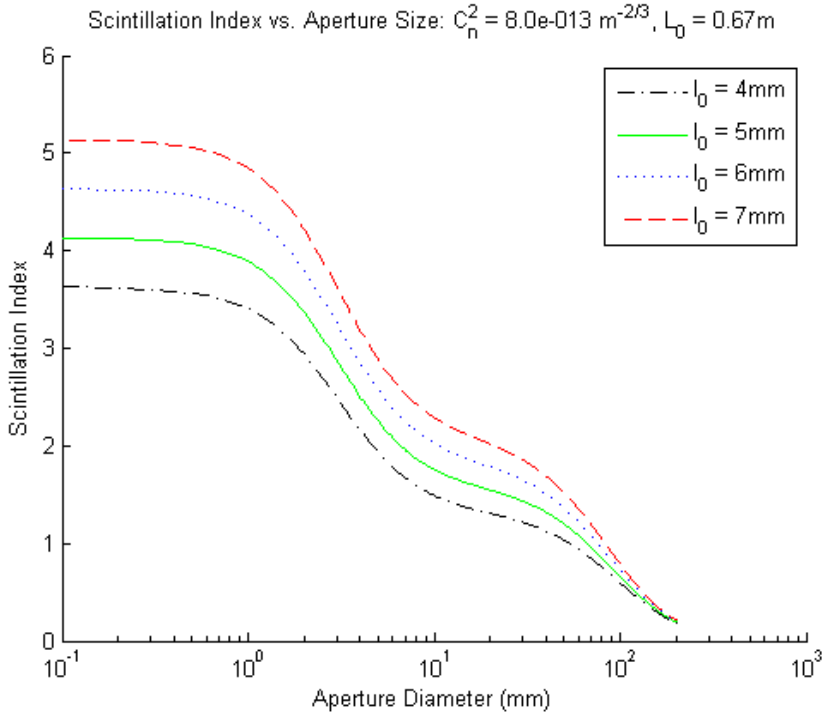

Figure 2 The scintillation index as a function of aperture diameter for a fixed range, outer scale L_0 and structure constant C_n^2. Various inner scale values are taken to illustrate the overall effect.

In earlier papers [1-4] we reviewed published C_n^2 data and presented new data [3] that support a daytime altitude-dependent $h^{-4/3}$ behavior of C_n^2 up to around 1-2 km above ground level, where h denotes altitude. We also described measurements of irradiance fluctuations (i.e., scintillation index) made on a beacon laser transmitted from an aircraft to a mountain top in Nevada at a range of roughly 100 km [4]. From these measurements, weighted path-average values of the three atmospheric parameters C_n^2, l_0, and L_0 were determined by making a comparison of the measured aperture-averaged scintillation index from three distinct aperture diameters with well known theoretical models [5].

3.1 HAP Profile Model for C_n^2

Calculations of optical turbulence effects on an optical wave propagating through the atmosphere are necessary for modeling purposes and also understanding the results of experimental data involving the beam. Because such calculations rely heavily on optical turbulence models, it is important to have a good understanding of the basic behavior of C_n^2 for the geographic area of interest. In applications involving propagation across a homogeneous terrain along a horizontal path it is common to assume that the structure parameter C_n^2 remains constant along the path. This constant value can be reasonably estimated by using an instrument called a scintillometer that characterizes the same path or a nearby parallel path. If propagation is along a vertical or slant path, it is necessary to use certain analytic or numerical models of optical turbulence to describe changes in C_n^2 as a function of altitude. These are known as C_n^2 profile models and typically represent an average value of C_n^2 at a given altitude, based on various measurements made over several years.

Many of the C_n^2 profile models developed over the years are discussed in the article by Beland [6]. Here we concentrate on a variation of the HV model [6], called the HAP model [4], viz.,

$$C_n^2(h) = M\left[0.00594\left(\frac{w}{27}\right)^2\left(\frac{h+h_s}{10^5}\right)^{10}\exp\left(-\frac{h+h_s}{1000}\right) + 2.7\times10^{-16}\exp\left(-\frac{h+h_s}{1500}\right)\right] + C_n^2(h_0)\left(\frac{h_0}{h}\right)^p, \quad h > h_0, \tag{1}$$

where h_s is the height of ground above sea level, h_0 represents height above ground of the TASS instrumentation, $C_n^2(h_0)$ is the average refractive index structure parameter at h_0, w is high-altitude average wind speed (typically 21 m/s), and altitude h varies from the reference height h_0 above ground of the TASS instrumentation to the maximum height of the beam (or transmitter) above ground. The parameter M characterizes an average value of the random background turbulence at altitudes generally above 1 km.

3.2 Algorithm for Finding HAP Parameters

The model for the power-law parameter p in the last term of the HAP model (1) is dependent on the temporal hour of the day that measurements are made. This requires knowledge of the local times at which sunrise (RISE) and sunset (SET) occur. The time between sunrise and sunset is equally divided into 12 temporal hours (TH) by the relationship

$$\mathrm{TH} = \frac{\mathrm{TIME} - \mathrm{SUNRISE}}{\mathrm{TP}}; \quad \mathrm{TP} = \frac{\mathrm{SUNSET} - \mathrm{SUNRISE}}{12} \tag{2}$$

where the local time is designated by TIME. For the Hollister and China Lake sites, we calculated the power law p between sunrise and sunset by the following rule:

$$p = \begin{cases} -0.11(12-\mathrm{TH})^2 + 1.83(12-\mathrm{TH}) - 6.22, & 0.75 < \mathrm{TH} < 3.5 \\ 1.45 - 0.02(\mathrm{TH}-6)^2, & 3.5 < \mathrm{TH} < 8.5 \\ -0.048 \cdot \mathrm{TH}^2 + 0.68 \cdot \mathrm{TH} - 1.06, & 8.5 < \mathrm{TH} < 11.25 \end{cases} \tag{3}$$

Based on (3), the power law p transitions between a value near 0.5 at TH = 0.75 up to a value near 1.45 at TH = 6 and then down to a value near 0.5 at TH = 11.25. For nighttime measurements between sunset and sunrise, it is expected that $p = 2/3$ [3,4,6]. At this point it is not clear whether the result of (3) is a universal result or not.

From the weighted path-average values of the refractive-index structure parameter C_n^2 and measured aperture-averaged scintillation values, an algorithm developed by UCF can determine the parameters M and $C_n^2(h_0)$ of the HAP C_n^2 profile model. This is done by calculating the aperture-averaged weak turbulence scintillation index as derived from the Kolmogorov spectrum [5], i.e.,

$$\sigma_I^2(D_R) = 8\pi^2 k^2 \int_0^L \int_0^\infty \kappa \Phi_n(\kappa, z) \exp\left(-\frac{D_R^2 z^2}{16L^2}\right) \left\{1 - \cos\left[\frac{\kappa^2}{k} z\left(1 - z/L\right)\right]\right\} d\kappa dz \tag{4}$$

where z is distance along the propagation path, D_R is a chosen receiver aperture diameter (more than one is required), and the Kolmogorov spectrum is defined by

$$\Phi_n(\kappa, z) = 0.033 C_n^2(z) \kappa^{-11/3} \tag{5}$$

In this analysis we ignore inner and outer scale parameters. By matching the results of the integration in (4) using the weighted path-average C_n^2 value for $C_n^2(z)$ in (5) and then repeat using the HAP model (1), we can determine both M and $C_n^2(h_0)$.

3.3 Calculating Inner Scale and Outer Scale Parameters

To calculate the inner scale and outer scale profiles as a function of altitude, we use the modified refractive-index spectrum described by [5]

$$\Phi_n(\kappa,h) = \underset{\text{HAP}}{0.033 C_n^2(h)\kappa^{-11/3}} \left[1 + 1.802\left(\frac{\kappa}{\kappa_l(h)}\right) - 0.254\left(\frac{\kappa}{\kappa_l(h)}\right)^{7/6} \right] \underbrace{\exp\left(-\frac{\kappa^2}{\kappa_l^2(h)}\right)}_{\text{Inner scale term}} \underbrace{\left[1-\exp\left(-\frac{\kappa^2}{\kappa_0^2(h)}\right)\right]}_{\text{Outer scale term}} \tag{6}$$

$$0 \le \kappa < \infty; \quad \kappa_l(h) = \frac{3.3}{l_0(h)}, \quad \kappa_0(h) = \frac{8\pi}{L_0(h)} \text{ (scin) or } \frac{2\pi}{L_0(h)}.$$

Then, with the HAP $C_n^2(h)$ profile model, we use the following expressions for the outer scale and inner scale:

$$\textit{Outer scale}: \quad L_0(h) = \frac{10 L_0(h_0)}{1+\left(\frac{h-7500}{2500}\right)^2}; \quad L_0(h_0) = \text{outer scale at } h_0 \text{ [meters]}$$

$$\textit{Inner scale}: \quad l_0(h) = \frac{10 l_0(h_0)}{1+\left(\frac{h-7500}{2500}\right)^2}; \quad l_0(h_0) = \text{ inner scale at } h_0 \text{ [meters]}$$

The upper expression for outer scale is based on numerous measurements made at various locations around the world [7]. The lower expression for inner scale is a simple model (not based on measurements) taken as a percentage of the outer scale expression.

Based on a spherical wave model for the beacon beam, the scintillation index for a point aperture is described by [5]

$$\sigma_I^2(0) = \exp\left[\sigma_{\ln X}^2(l_0) - \sigma_{\ln X}^2(L_0) + \frac{0.51\sigma_{SP}^2}{\left(1+0.69\sigma_{SP}^{12/5}\right)^{5/6}} \right] - 1 \tag{7}$$

where $\sigma_{\ln x}^2(l_0)$ and $\sigma_{\ln x}^2(L_0)$ are small scale irradiance fluctuations, and σ_{SP}^2 is the weak fluctuation Rytov expression for the spherical wave scintillation index with inner scale. By calculating the predicted scintillation index for a point aperture (7) using the path-average C_n^2, path-average inner and outer scale values in the spectrum (6) and comparing with that produced by the HAP $C_n^2(h)$ model together with the above expressions for inner and outer scale as a function of altitude, we can estimate ground level values of inner scale and outer scale.

4.0 FREE SPACE OPTICAL COMMUNICATION SYSTEMS

Free space optical communications (FSOC) has become an important application area because of the increasing need for larger bandwidths and high-data-rate transfer of information that is available at optical wavelengths. Although early interests concentrated

largely on higher and higher data rates afforded by optical systems over radio frequency (RF) systems, some of the greatest benefits of FSO communication may be: (*i*) less mass, power, and volume as compared with RF systems, (*ii*) the intrinsic narrow-beam/high-gain nature of laser beams, and (*iii*) no regulatory restrictions for using frequencies and bandwidths.

4.1 Background

FSOC is a line-of-sight technology that uses lasers to provide optical bandwidth connections without requiring fiber-optic cable. Only 5 percent of the major companies in the United States are connected to fiber-optic infrastructure (backbone), yet 75 percent are within one mile of fiber (known as the "Last Mile Problem"). As bandwidth demands increase and businesses turn to high-speed LANs (local area networks), it becomes more frustrating to be connected to the outside world through lower-speed connections such as DSL (digital subscriber line), cable modems, or T1s (transmission system 1).

Typical laser wavelengths considered for FSOC systems are 850 and 1550 nanometers (nm). Low-power infrared lasers, which operate in an unlicensed electromagnetic-frequency band either are eye-safe or can be made to operate in an eye-safe manner. However, limiting the power emitted by a laser restricts the range of applicability. Depending on weather conditions, FSOC links along horizontal near-ground paths can extend from a few hundred meters up to several kilometers or more—far enough to get broadband traffic from a backbone to many end users and back. For aircraft-to-ground or aircraft-to-aircraft links the ranges can be up to 100 km or more. Because bad weather (thick fog or clouds, mainly) can severely curtail the reach of these line-of-sight devices, each optical transceiver node, or link head, can be set up to communicate with several nearby nodes in a network arrangement. This "mesh topology" can ensure that vast amounts of data will be relayed reliably from sensor suites to central control centers and users.

Susceptibility to fog has slowed the commercial deployment of near-ground FSOC systems. It turns out that fog (and perhaps rain and snow) considerably limits the maximum range of an FSOC link. Because fog causes significant loss of received optical power, a practical FSOC link must be designed with some specified "link margin," i.e., an excess of optical power that can be engaged to overcome foggy conditions when required. Under ideal clear-sky conditions, the absolute reliability of a laser communication link through the atmosphere is still physically limited by absorption of atmospheric constituents and the constantly present atmospheric turbulence. For a given link margin, it becomes meaningful to speak of another metric—the link availability, which is based on the fraction of the total operating time that the link fails as a result of fog or other physical interruption. Link-availability objectives vary with the application.

FSOC technology started in the 1960s, but deleterious atmospheric effects on optical waves together with the invention of optical fibers in the early seventies caused a decline in its immediate use. FSOC systems today can provide high-speed connections between

buildings, between a building and the optical fiber network, or between ground and a satellite. Moreover, a FSOC system can often be installed in a matter of days or even hours in some cases, whereas it can take weeks or months to install an optical fiber connection. Now, because of the growing demand for access to high-data-rate connections all over the world and the inherent limitations of optical fiber networks in certain environments, there is renewed interest in FSOC.

Some additional common types of FSOC channels that are of current interest are cited below with a brief description of primary atmospheric effects:

> *Aircraft-ground:* Laser communications to the ground from an aircraft are disrupted mostly by the atmospheric turbulence closest to the ground receiver. The primary concerns for downlink propagation paths are *scintillation* and *angle-of-arrival fluctuations***.** Also, aircraft *boundary layer effects* due to platform speed may need to be addressed.
>
> *Ground-aircraft:* A transmitted laser beam from the ground to an aircraft is disrupted mostly by atmospheric turbulence near the transmitter. The primary concerns for an uplink path are *beam spreading*, *scintillation*, and *beam wander*.
>
> *Aircraft-aircraft:* Although the aircraft is above much of the natural atmospheric ground-induced turbulence, atmospheric turbulence is still a concern and aircraft *boundary layer effects* due to platform speed may also need to be addressed.

4.2 FSOC System Performance Modeling

An FSOC link budget provides the ability to predict system performance under a wide range of conditions and enables effective operation planning. It is an extremely valuable tool but requires underlying models that accurately capture system and component performance under a wide range of environmental conditions. Perhaps the most fundamental component of a link budget is the atmospheric optical channel model. In many FSOC systems it may also be necessary to develop an adaptive optics (AO) gain model and an optical automatic gain controller (OAGC) model. The AO system may consist of only tip-tilt corrections or, for more sophisticated systems, include a number of higher-order AO correction modes. The atmospheric model captures the impact of the atmosphere on the power into the receiver aperture while the AO gain model addresses the various atmospheric perturbations and defines the extent to which those effects can be mitigated in order to focus light into an optical fiber. The OAGC model then defines the ability of the system to convert the light into a stable and usable optical signal to be passed along to the modem. In addition to these methods, it may still be necessary to introduce other mitigating techniques such as a forward error control (FEC) coding scheme or spatial diversity of transmitters and/or receivers.

4.3 Statistical Performance Measures

The reliability of a FSOC system can be deduced from the analysis of several statistical performance measures:

- *Strehl Ratio* (SR)—defined by the ratio of the long-term mean irradiance of the laser beam in atmospheric turbulence to that in free space. If the receiver is located in the far-field of the transmitter, the SR in the receiver plane (RP) can be expressed in the form

$$\mathrm{SR}_{\mathrm{RP}} = \frac{1}{\left[1+\left(D_{\mathrm{Tx}}/r_{0\mathrm{T}}\right)^{5/3}\right]^{6/5}}; \quad \underbrace{\left\{= \frac{1}{\left[1+0.052\left(D_{\mathrm{Tx}}/r_{0\mathrm{T}}\right)^{5/3}\right]^{6/5}}\right\}}_{\text{SR with 35 mode AO correctiom}} \tag{8}$$

where D_{Tx} is the aperture diameter of the transmitter and $r_{0\mathrm{T}}$ is the Fried parameter in the plane of the transmitter. The maximum value of the SR is unity in free space. In the detector plane (DP), the resulting SR is

$$\mathrm{SR}_{\mathrm{DP}} = \frac{1}{\left[1+\left(D_{\mathrm{Rx}}/r_{0\mathrm{R}}\right)^{5/3}\right]^{6/5}}; \quad \underbrace{\left\{= \frac{1}{\left[1+0.052\left(D_{\mathrm{Rx}}/r_{0\mathrm{R}}\right)^{5/3}\right]^{6/5}}\right\}}_{\text{SR with 35 mode AO correctiom}} \tag{9}$$

where D_{Rx} is the aperture diameter of the receiver and $r_{0\mathrm{R}}$ is Fried's parameter in the plane of the receiver. For a beam propagating a distance L in the positive z direction, the two Fried parameters are defined by

$$\begin{aligned} r_{0\mathrm{T}} &= \left[0.423k^2\int_0^L C_n^2(z)\left(1-\frac{z}{L}\right)^{5/3}dz\right]^{-3/5} \\ r_{0\mathrm{R}} &= \left[0.423k^2\int_0^L C_n^2(z)\left(\frac{z}{L}\right)^{5/3}dz\right]^{-3/5} \end{aligned} \tag{10}$$

where k is optical wave number.

- *Power in the bucket* (PIB)—the average power that enters a receiver aperture. If P_{Tx} represents the laser power at the exit aperture of the transmitter, the average PIB at the receiver is

$$\langle \mathrm{PIB} \rangle = P_{\mathrm{Tx}} \cdot \frac{D_{\mathrm{Rx}}^2}{8W^2} \cdot \tau_{\mathrm{atm}} \cdot \tau_{\mathrm{opt}} \cdot \mathrm{SR}_{\mathrm{RP}}; \quad D_{\mathrm{Rx}} \le 2\sqrt{2}W \tag{11}$$

where W is the free-space Gaussian beam radius of the laser beam in the receiver plane, τ_{atm} is the atmospheric transmission loss, and τ_{opt} is the

receiver transmission loss up to the AO subsystem. An alternative way to express the mean PIB in the far field is by

$$\langle \mathrm{PIB} \rangle = P_{\mathrm{Tx}} \cdot \frac{A_{\mathrm{Tx}} A_{\mathrm{Rx}}}{(\lambda L)^2} \cdot \tau_{\mathrm{atm}} \cdot \tau_{\mathrm{opt}} \cdot \mathrm{SR}_{\mathrm{RP}}; \quad D_{\mathrm{Rx}} \le 2\sqrt{2}W \tag{12}$$

where A_{Tx} and A_{Rx} denote the areas, respectively, of the transmitter aperture and receiver aperture and $\lambda = 2\pi / k$ is wavelength.

- *Power in the fiber* (PIF)—when an optical fiber is located in the detector plane, then $\langle \mathrm{PIF} \rangle$ represents the average power that enters the fiber core. It's maximum value is

$$\langle \mathrm{PIF} \rangle = \langle \mathrm{PIB} \rangle \cdot \tau_{\mathrm{opt}} \cdot \tau_{\mathrm{fiber}} \cdot \mathrm{SR}_{\mathrm{DP}} \tag{13}$$

where τ_{fiber} represents the fiber loss due to the presence of a circulator.

For aircraft-to-aircraft or aircraft-to-ground links, the aero-optic boundary layer around the aircraft can introduce fluctuations in the beam other than those caused by atmospheric turbulence between the aircraft and the optical receiver. These aero-optic-induced fluctuations in the beam may reduce the average collected power even further than represented above. In some cases it may be possible to model the aero-optic boundary layer as a thin random phase screen from which additional beam spreading can be estimated.

4.4 Hybrid FSO/RF Systems

Recent efforts at the Defense Advanced Research Projects Agency (DARPA) and Air Force Research Laboratory (AFRL) show that the needed performance to emulate a FSOC system can be achieved by a hybrid system that incorporates FSOC, directional RF, and adaptive networking. Key results were reported regarding the 2006/2007 experiments conducted under the AFRL Integrated RF/Optical Networked Tactical Targeting Networking Technologies (IRON-T2) Program [8-12]. The tests for the AFRL IRON-T2 Program, culminating in IRON-T2 2008 [12], demonstrated the efficacy of a combined optical/RF communications system. Test data indicated that the FSOC technologies and hybrid approach could support reliable multi-Gigabit links under a wide range of day and night operating conditions. When atmospheric conditions, such as fog and clouds, denied optical communication, lower rate RF connectivity could sometimes be maintained if ducting and accompanying multipath interference were absent. Significant deleterious multipath effects occurred most often on low-angle RF links in the presence of temperature inversions. Varying atmospheric conditions caused one or other spectrum channel to fail, or both, or neither. The lesson learned was that no all-weather, all situation communications connectivity exists, but that a combined optical/RF communications system has greater availability than either one alone. In addition,

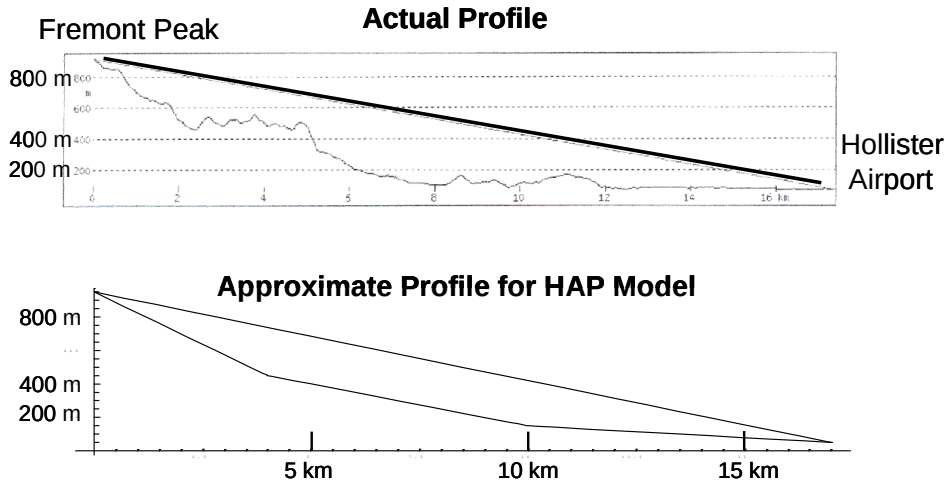

enhanced equalization subsystems in the RF domain can alleviate some multipath interference. Moreover, operations planning can mitigate link failures by adjusting flight trajectories based on outage prediction and detection.

DARPA and AFRL have since leveraged the IRON-T2 results to further research hybrid FSO/RF system performance and design under the DARPA Optical RF Communications Adjunct (ORCA) Program and follow-on, Free space Optical Experimental Network Experiment (FOENEX) Program. The intent of the ORCA/FOENEX Programs was to design, build, and test a prototype hybrid electro-optical and RF airborne backbone network. The IP-based hybrid FSO/RF network was designed to provide the capabilities and performance needed for tactical reach-back and data dissemination applications. Airborne nodes were expected to communicate between each other, up to ranges of 200 km at nominal altitudes of 25,000 ft or higher, while air-to-ground links were to achieve up to a 50 km slant range. As noted in the 2009 IEEE article [8], the major challenges for establishing a hybrid FSO/RF airborne communications capability are overcoming atmospheric turbulence over long ranges and low slant angles and mitigating multipath in low altitude RF.

5. DATA ANALYSIS AT HOLLISTER

During June 7-9, 2011 measurements were made on the FOENEX laser beam (1550 nm) transmitted over a 17-km path between a ground station at Hollister Airport and a ground station on Fremont Peak. The FOENEX data beam was transmitted from a 10-cm aperture and received by a 10-cm aperture in both directions. A parallel test was conducted by a University of Central Florida (UCF) team using the laser beacon transmitted from the ground station at Hollister Airport to Fremont Peak. The beacon beam was operating at 780 nm from a 2.54-cm transmitter aperture with a large beam divergence angle. The small aperture and large divergence angle permitted UCF to treat the beacon as coming from a point source (i.e., a spherical wave). The purpose of the UCF testing was to characterize the atmospheric channel between the ground station at Hollister Airport and Fremont Peak by determining weighted path-averaged values of the refractive-index structure parameter C_n^2, the inner scale of turbulence l_0, and the outer

scale of turbulence L_0. This was accomplished with a three-aperture scintillometer system (TASS) developed by UCF for long ranges. From the weighted path-average C_n^2 values, a C_n^2 profile model as a function of altitude *h* was constructed which provided ground-level C_n^2 values at 1-1.5 m above ground [i.e, $C_n^2(h_0)$ in Eq. (1)] and high-altitude background turbulence levels for the profile model [parameter *M* in Eq. (1)].

The ground profile for the propagation path between Hollister Airport and Fremont Peak is shown in Fig. 3 along with the piecewise linear approximation used by UCF to make the calculations for the HAP model.

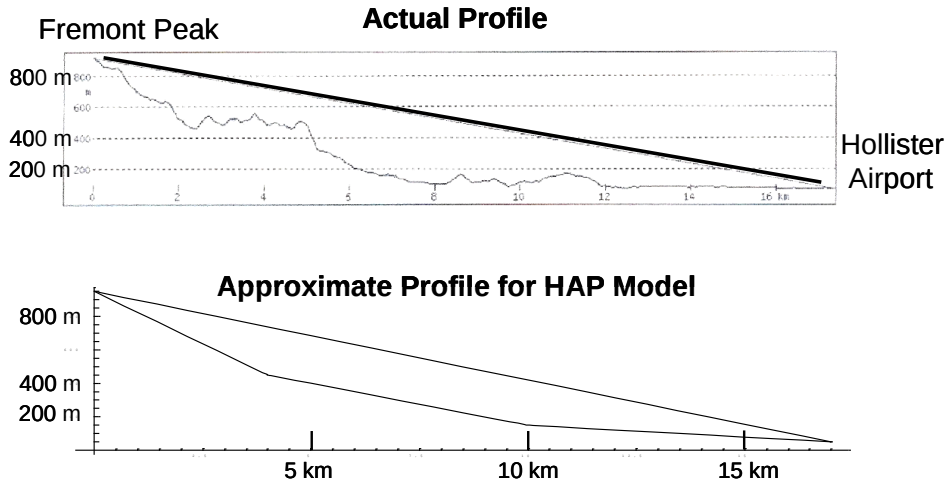

Figure 3 Ground profile (upper) and UCF piecewise linear approximation (lower) between Hollister Airport and Fremont Peak.

5.1 UCF Fremont Peak Setup

The UCF and AOptix instrumentation setup on Fremont Peak is shown in Fig. 4. The UCF TASS instrument is placed near the AOptix node and GPS unit so as to be in the footprint of the beacon beam. The view down to Hollister Airport is shown in Fig. 5.

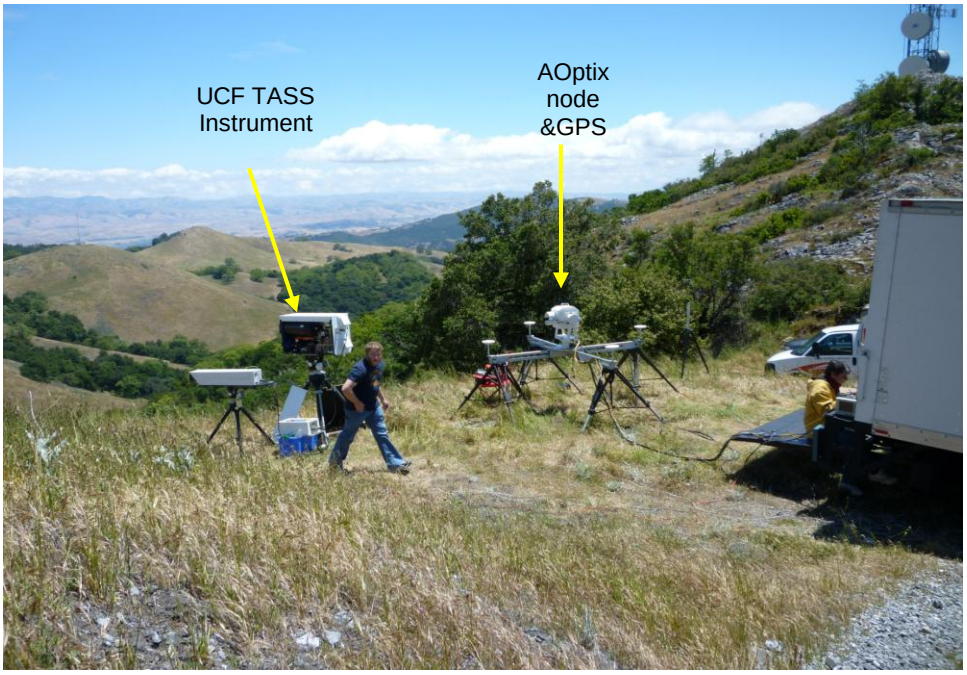

Figure 4 Instrument placement on Fremont Peak.

Atmospheric conditions were fairly consistent over all three days of testing (June 7-9). However, the top of Fremont Peak was in a cloud layer each day until ~ 8:00 am local time (PST), and the line-of-sight (LOS) to Hollister Airport was typically blocked by cloud layering until around 11:00 am each day. In addition to the UCF instrument for measuring atmospheric conditions, a BLS 900 Scintec scintillometer was positioned at Hollister Airport by APL to measure local C_n^2 ground conditions. The Scintec BLS 900 scintillometer provided a basis of comparison with the UCF estimation of local C_n^2 values at 1.5 m above the ground based on the C_n^2 profile model. However, the BLS 900 instrument was placed only at the Hollister Airport site whereas the UCF estimated values represent average C_n^2 values at 1.5 m altitude from Fremont Peak all along the 1.5 m ground path down to Hollister Airport.

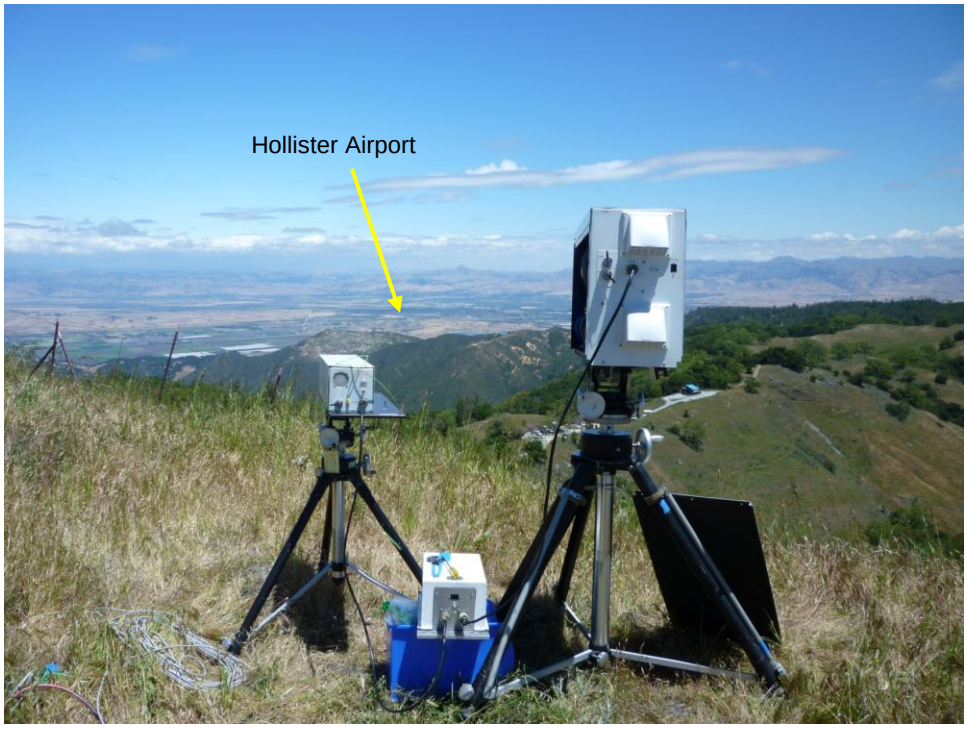

Figure 5 UCF instrumentation view from Fremont Peak down to Hollister Airport.

5.2 TASS Path-Averaged Values

Irradiance data were measured using three telescopes on a tripod (TASS) to capture the beacon beam from which aperture-averaged scintillation values were calculated. The aperture diameters of the telescopes were 7 cm, 12 cm, and 27.2 cm. From a mathematical model of the scintillation as measured with three apertures the inverse problem is solved for the parameters that created the scintillation. The general procedure for processing this data is essentially the same as described in Ref. [4]. Namely, the current software running the TASS uses a complex two-step minimization method with the downhill Simplex algorithm being used during both steps. The first step essentially determines the path-average C_n^2 parameter while the latter step determines inner scale and outer scale. The minimization is repeated 13 times, each time with a different seed. All outcomes that converge on a solution are reported by the algorithm. Also, the instrument was tested and calibrated prior to the Phase 0 testing at Hollister.

Scintillation data were collected by UCF on June 7, 6:30-7:30 pm (PST), June 8, 1:00-2:00 pm (PST) and 5:10-6:15 pm (PST), and on June 9, 12:15-1:40 pm (PST). The weighted path-average C_n^2 results from those measurements along with a 1-2 hour overall average are shown in Figs. 6-8. Note that the path-average C_n^2 data were fairly consistent from day to day without regard to time of day. For example, on June 7 the overall C_n^2 average was 2.22×10^{-15} $m^{-2/3}$, on June 8 the overall average was 2.29×10^{-15} $m^{-2/3}$ (1:00-2:00 pm) and 1.94×10^{-15} $m^{-2/3}$ (5:10-6:15 pm), and on June 9 the overall average was 2.08×10^{-15} $m^{-2/3}$. As shown below, however, the C_n^2 data near the ground (1.5 m) as determined by the BLS 900 scintillometer were considerably lower

in the late afternoon hours as compared with measurements earlier in the day. This behavior is consistent with the general diurnal behavior of C_n^2 during the day [6].

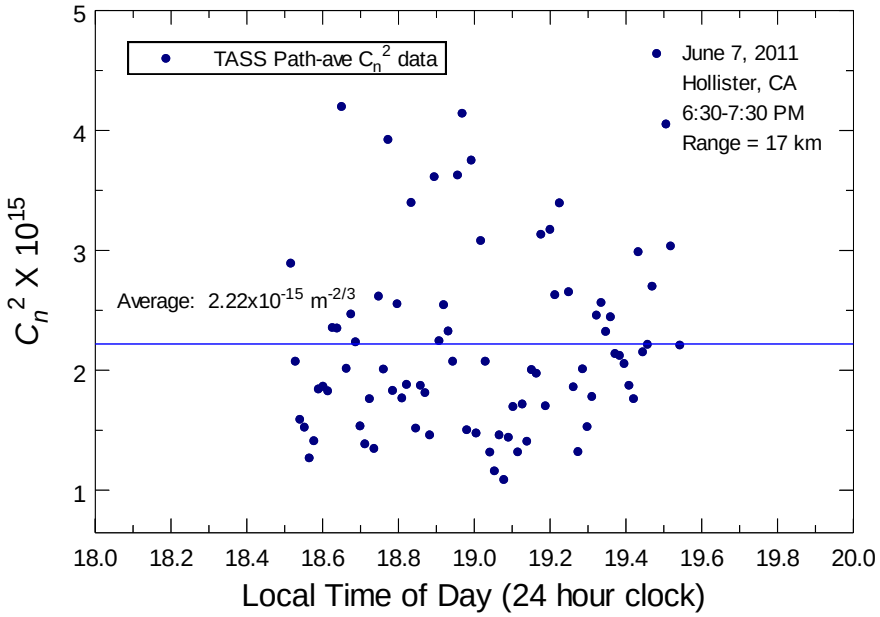

Figure 6 Weighted path-average values of C_n^2 from TASS as measured on June 7 between Hollister Airport and Fremont Peak. Averaging time was 44 s.

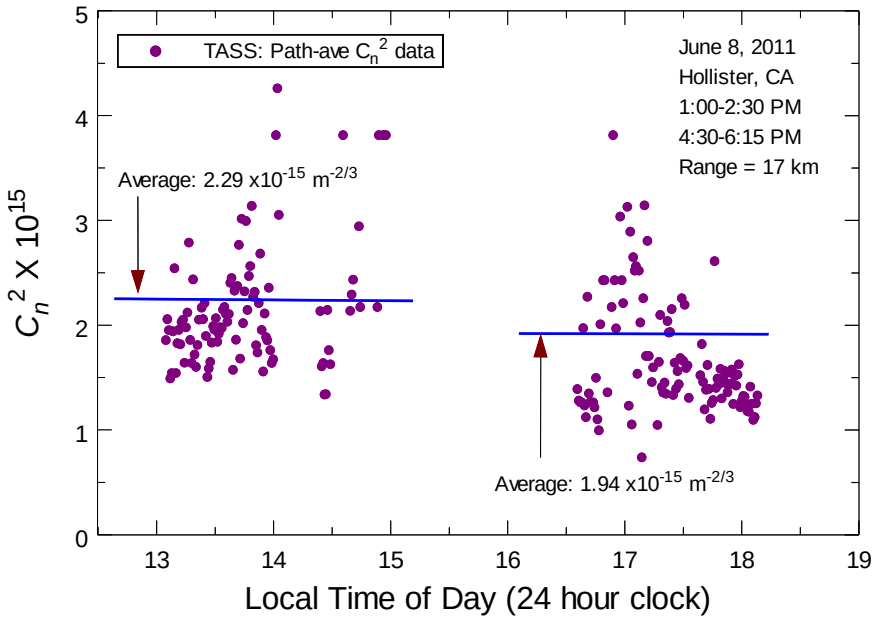

Figure 7 Same as Fig.6 for June 8.

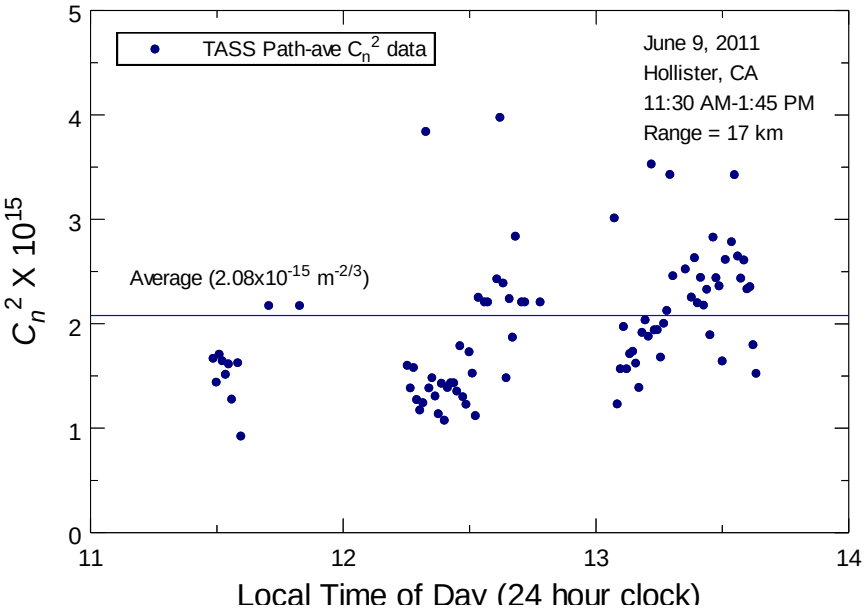

Figure 8 Same as Fig. 6 for June 9.

Weighted path-average inner scale values ranged over all three days mostly between 1 cm and 4 cm, although values up to 6 cm and greater were sometimes predicted by the algorithm. Outer scale values could not be properly determined because scintillation values were on the front peak of the curves shown in Fig. 1, prior to where outer scale effects begin to show influence.

5.3 Results for the HAP Model Parameters

The results of matching the predicted $C_n^2(h_0)$ near the ground at height h_0 above ground with similar results from the BLS 900 Scintec scintillometer are shown in Figs. 9-12 below. In Fig. 9 we present 1-min averages of data (filled red triangles) from the BLS 900 Scintec scintillometer located at Hollister Airport. This data were taken during the late afternoon from 6:30-7:30 pm (PST) on June 7. The blue open circles represent the estimated $C_n^2(h_0)$ values based on the HAP model derived from UCF path-average measurements. The solid curve represents the average $C_n^2(h_0)$ value derived from a 1-2 hour overall weighted path-average C_n^2 for that time period. In Figs. 10, 11 and 12 we show similar data as that in Fig. 9 for the days June 8 and June 9. As in Fig. 9, the comparison of C_n^2 values between the BLS 900 instrument and the estimated values from the HAP model are generally in good agreement.

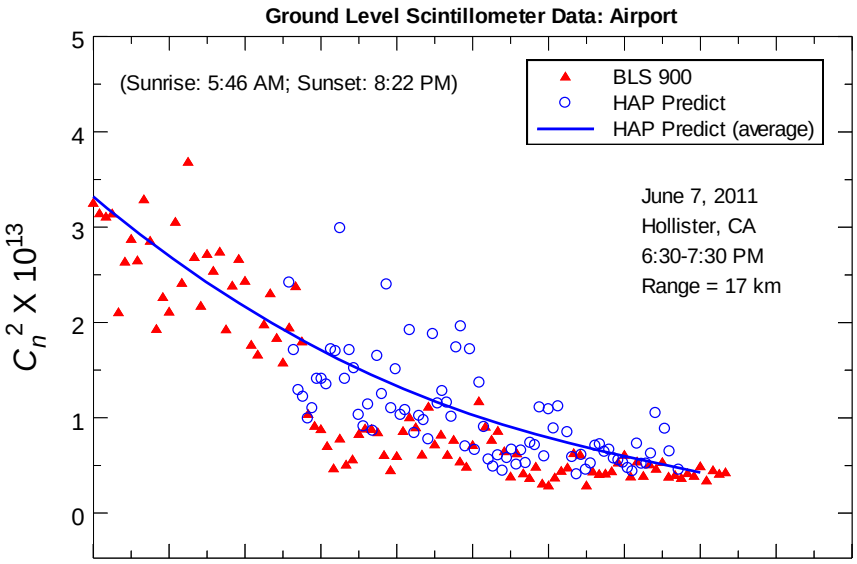

Figure 9 Measured data (filled triangles) from the BLS 900 scintillometer based on 1-min averages of C_n^2 at 1.5 m above the ground at Hollister Airport on June 7. The open circles are estimated values from the UCF HAP model and the solid line is the 1-2 hour overall HAP model average.

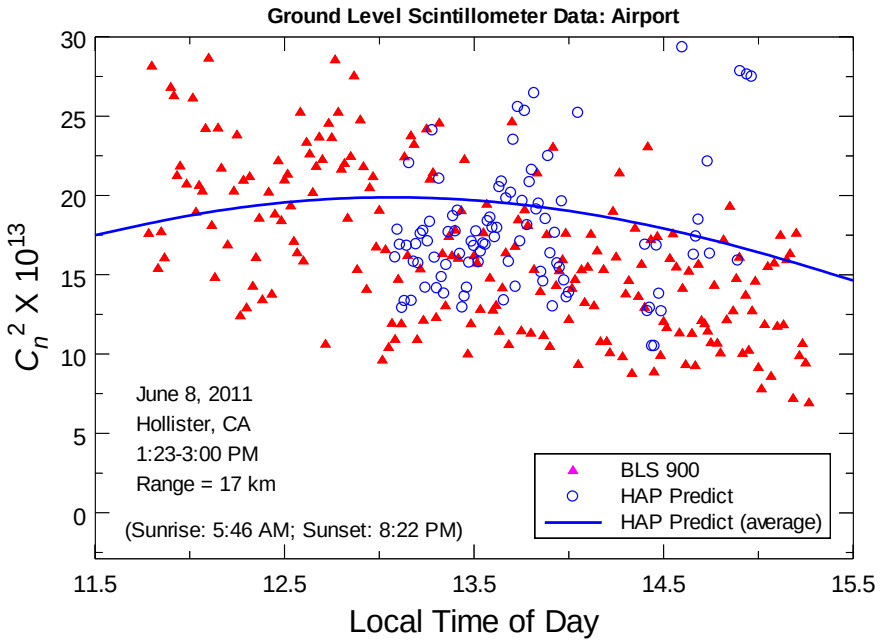

Figure 10 Same as Fig. 9 for June 8.

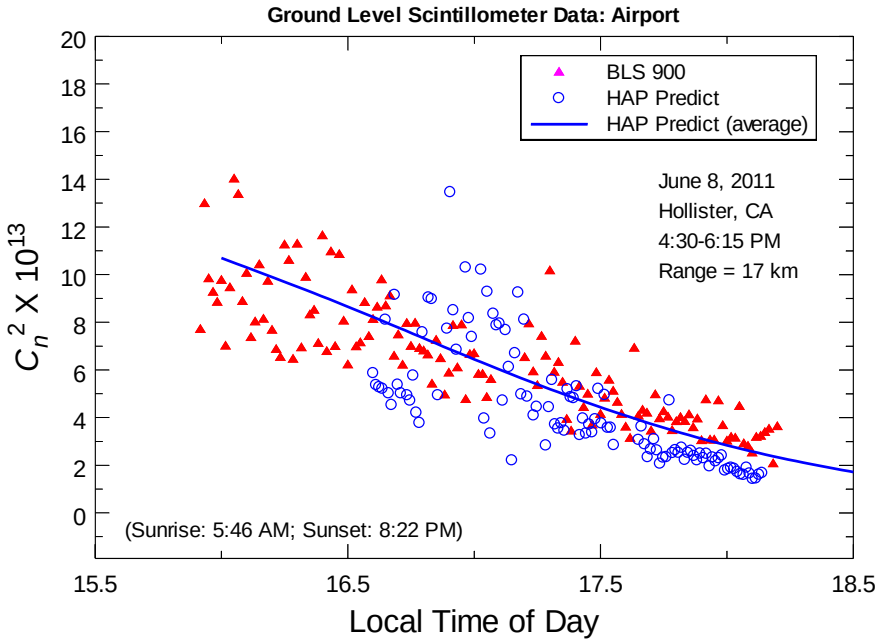

Figure 11 Same as Fig. 9 for June 8.

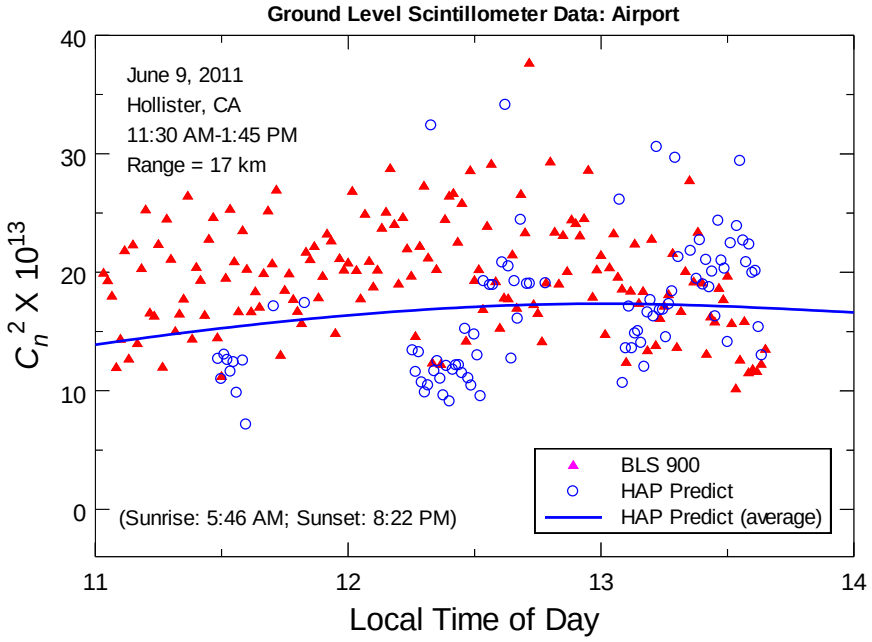

Figure 12 Same as Fig. 9 for June 9.

5.4 Fried Parameter from HAP Model

Once its parameters are determined, the HAP C_n^2 profile model can be used to estimate statistics of any other beam (same or different wavelength) along the same path or nearby path. To illustrate, let us assume we wish to calculate the Fried parameter r_0 for a collimated Gaussian beam operating at 1550 nm over the same 17-km path between Hollister Airport and Fremont Peak. Because the beam at the receiver is in the far field, the Fried parameter can be well estimated by the spherical wave expression

$$r_0 = \frac{2.1}{\left[1.46k^2 \int_0^L C_n^2(z)\left(\frac{z}{L}\right)^{5/3} dz\right]^{3/5}} \tag{14}$$

In Fig. 13 we plot the Fried parameter generated from (14) at both ends of the 17-km propagation path as a function of local time of day for data collected roughly every 5 min on June 8. In Fig. 14, we show the general behavior of Fried's parameter at both ends of the path with the assumption that the overall weighted path-average refractive-index parameter is the same nominal value $C_n^2 = 2.0\times10^{-15}$ m$^{-2/3}$ for all three days of testing. Although no data was actually taken before midday during the June 7-9 testing, we can use the nominal value of C_n^2 to estimate the Fried parameter over local time ranging from 9:00 am to 7:00 pm (PST). Here we see that the Fried parameter acts like the inverse of the C_n^2 diurnal behavior. That is, the Fried parameter takes on its minimum values in the middle part of the day and exhibits its largest values during the morning and late afternoon.

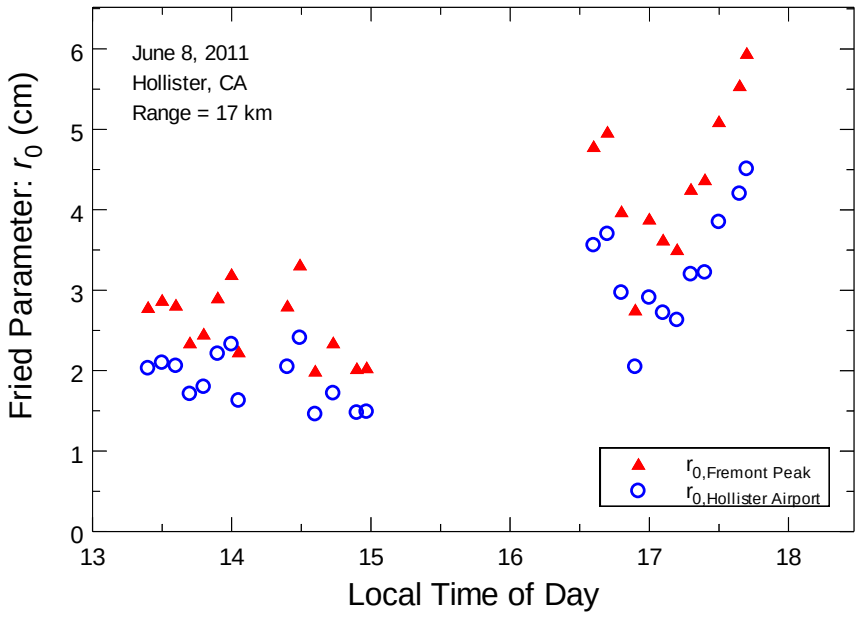

Figure 13 Estimated value of the Fried parameter at each end of the propagation path between Hollister Airport and Fremont Peak for data taken roughly every 5 min on June 8 during the time periods shown in the graph.

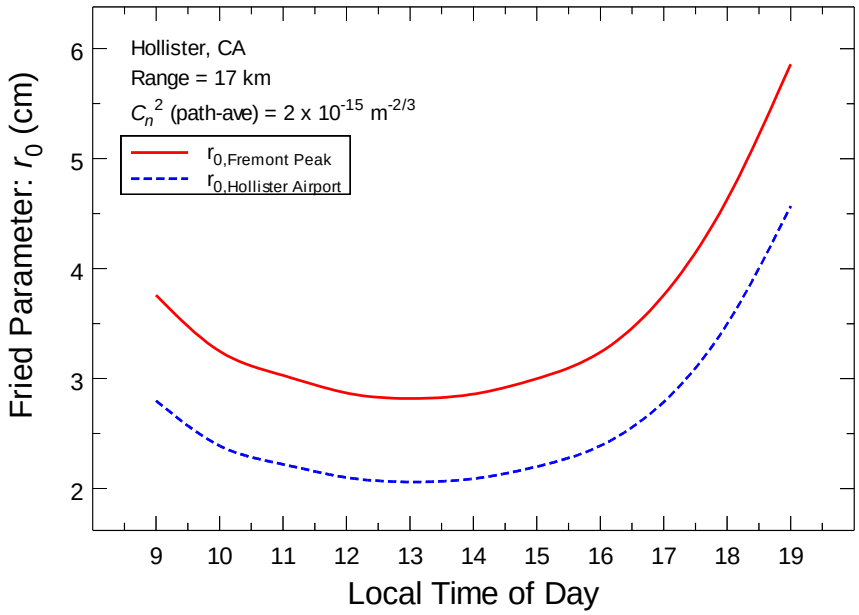

Figure 14 Estimated value of the Fried parameter at each end of the propagation path between Hollister Airport and Fremont Peak, assuming that the overall path-average C_n^2 value was a nominal constant value during the time period shown in the graph.

5.5 Data Beam Analysis: PIB and PIF

The data beam for the FOENEX FSOC system operates at 1.55 microns out of a 10-cm aperture. The receiver aperture is also 10 cm. The FSOC system operates in both directions so the analysis will be at both ends of the link. Of particular importance in our analysis is the determination of power in the bucket (PIB) and power in the fiber (PIF). PIB refers to the laser light that is actually captured by the receiver aperture and PIF refers to how much of that laser light gets into the optical fiber.

One deleterious effect of the atmosphere is that it causes additional beam spreading (beyond diffraction effects) at the Rx through "beam wander" (i.e., a random tilt angle) on the outgoing beam from the Tx. By invoking the principle of reciprocity, the associated beam wander at the Rx due to the atmosphere can be modeled as a random phase tilt at the Tx. By removing this random tilt at the Tx, called "tracking the beam," most of the beam wander effects from the atmosphere can be removed.

In addition to beam wander, the beam may also experience another random tilt known as angle-of-arrival (AOA) fluctuations at the Rx pupil plane. This AOA tilt will manifest itself as a larger (long-term) beam spot size at the entrance to the optical fiber that can result in a loss of available PIF. By incorporating a tip-tilt correction at the Rx, the resulting spot size at the fiber will be reduced to a "short-term" spot size close to the free space spot size and consequently lead to a larger PIF value. Consequently, our theoretical analysis of the data beam will generally involve two components of tip-tilt—that at the Tx due to beam wander and that at the Rx due to AOA fluctuations. A key feature of the FOENEX FSOC system is that the transmitter and receiver paths within the optical

hardware are reciprocal, each having adaptive optics (AO), thereby correcting both the transmitted beam and the received beam to maximize light coupling into the fiber.

Although beam wander and AOA are probably the main effects of the atmosphere that can be corrected by the AO subsystem, the AO subsystem that is employed in FOENEX is capable of correcting up to 35 Zernike modes. This additional mode correction can lead to an increase in PIF of several dB in some cases.

The actual times of testing at the Hollister site are given below:

- **June 7, 2011**
  - 2-3 PM local time (PST) (no UCF data)
  - 6:30-7:30 PM local time (PST)
  - UCF weighted path-average *mean*: $C_n^2 = 2.22 \times 10^{-15}\ \mathrm{m}^{-2/3}$

- **June 8, 2011**
  - 1-2 PM local time (PST)
  - 5:10-6:15 PM local time (PST)
  - UCF weighted path-average *mean*: $C_n^2 = 2.29 \times 10^{-15}\ \mathrm{m}^{-2/3}$, $C_n^2 = 1.94 \times 10^{-15}\ \mathrm{m}^{-2/3}$

- **June 9, 2011**
  - 12:15-1:40 PM local time (PST)
  - UCF weighted path-average *mean*: $C_n^2 = 2.08 \times 10^{-15}\ \mathrm{m}^{-2/3}$

PIB data measured from 6:30-7:30 pm on June 7 at the Hollister end of the path is shown in Fig. 15(*a*) whereas the corresponding PIF data at the same location and time is shown in Fig. 15(*b*). PIB values with and without full AO are deduced from the SR given in (8) and that for PIF from (9). Blue shaded areas represent AO utilized at both ends, red shaded areas represent Tx AO only, and green represents Rx AO only. The horizontal lines represent UCF average theoretical values for each of these situations. Here we see that the theoretical PIB matches the measured data quite well as does the PIF. Figure 16 represents the PIB and PIF data taken at the Fremont end of the link during the 6:30-7:30 pm timeframe on June 7. The color codes are the same as those in Fig. 15. In this case both PIB and PIF theoretical results are once again close to those measured. Atmospheric transmission loss was estimated at -1.5 dB.

Although we have good agreement between theoretical estimates and actual measured results for both PIB and PIF during the 6:30-7:30 pm timeframe on June 7, we found in general that this was not the case for other testing times. See, for example, Figs. 17 and 18 corresponding to data taken between 1:00-2:00 pm on June 8. We do point out, however, that theoretical PIB values with full AO on were always in good agreement with measured data during all testing times at the Hollister site (both ends of the link). This suggests that the full Tx AO subsystem was always effective. The PIF theoretical

values with both Tx and Rx AO turned on were generally higher than measured PIF data by as much as 6-15 dB (except on June 7 between 6:30 and 7: 30 pm as already noted).

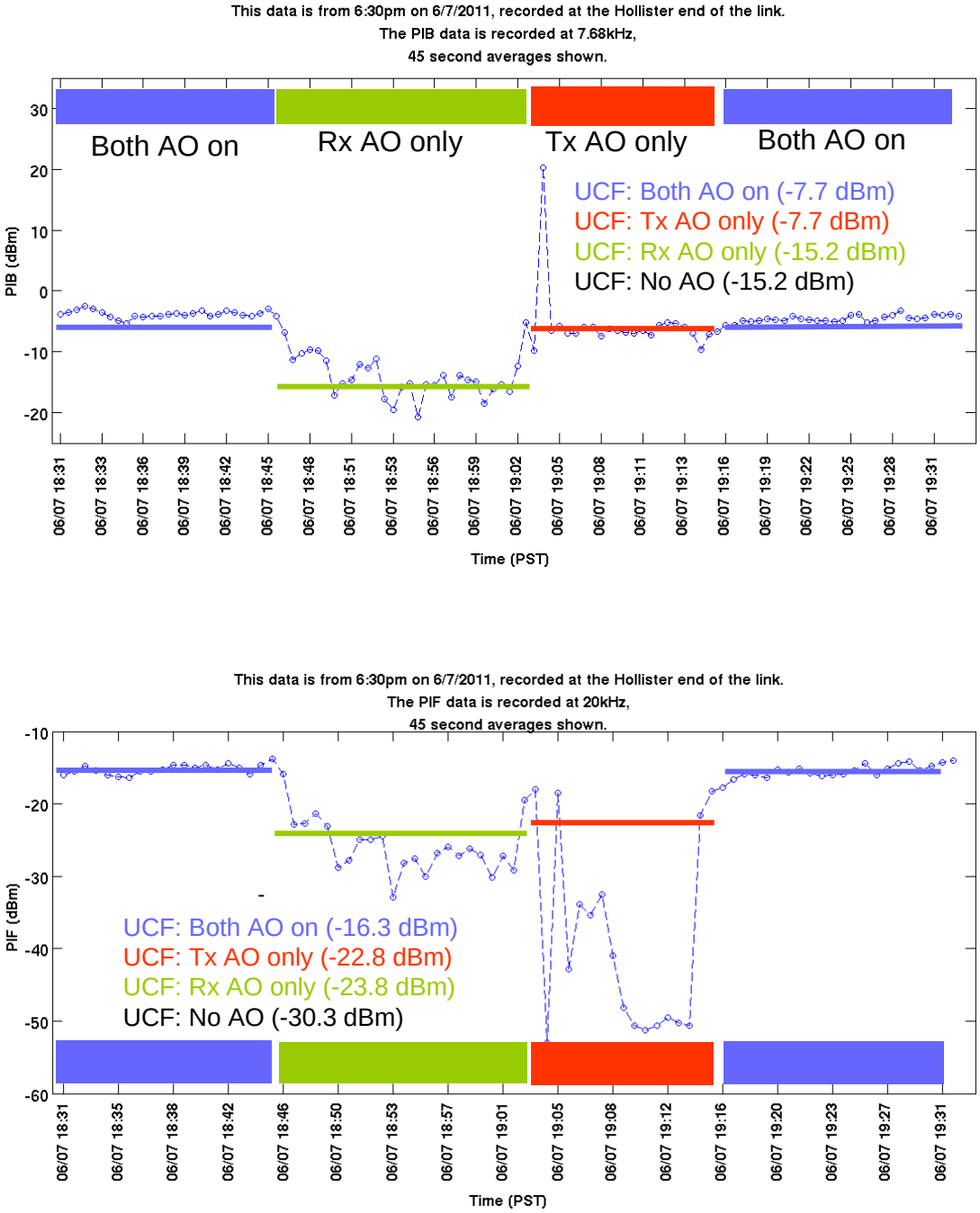

Figure 15 (*a*) PIB data taken during 6:30-7:30 pm on June 7 at the Hollister end of the path and (*b*) PIF data taken at the Hollister end of the path during the same time.

(a)

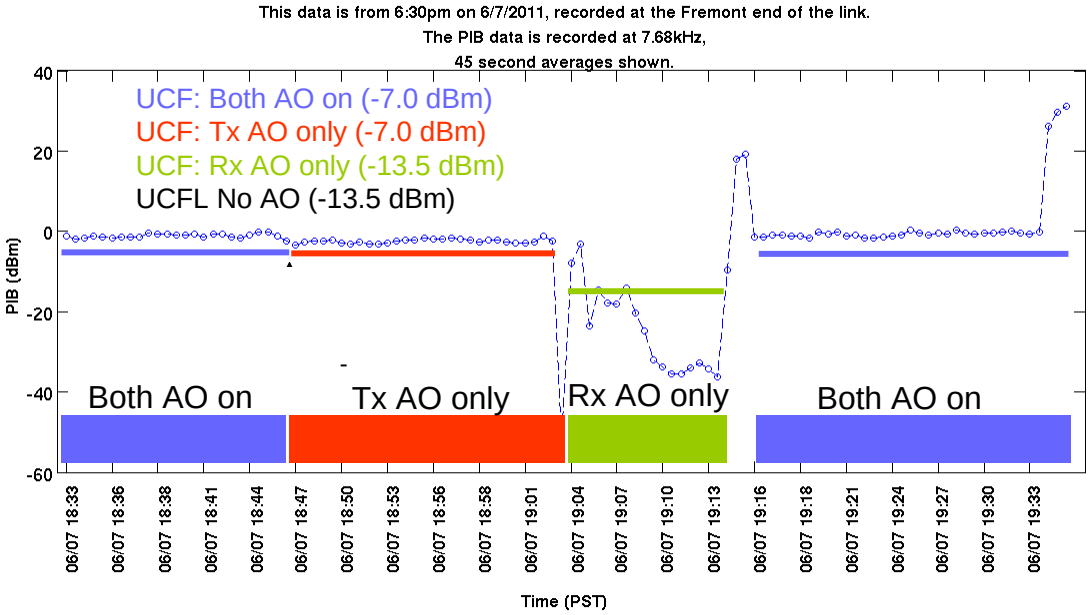

(b)

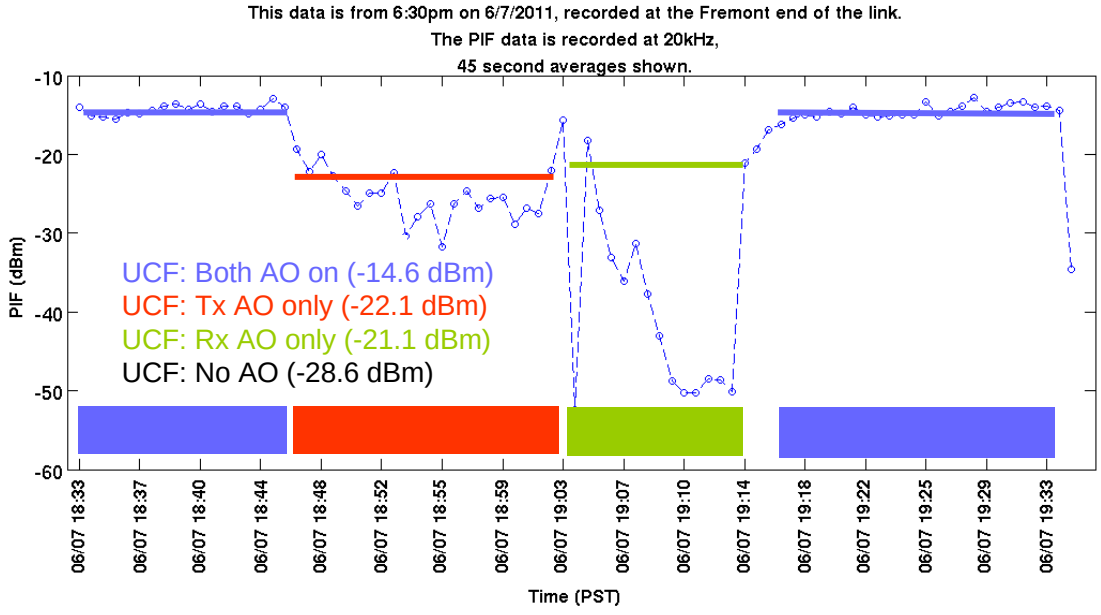

Figure 16 (*a*) PIB data taken during 6:30-7:30 pm on June 7 at the Fremont end of the path and (*b*) PIF data taken at the Fremont end of the path during the same time.

(a)

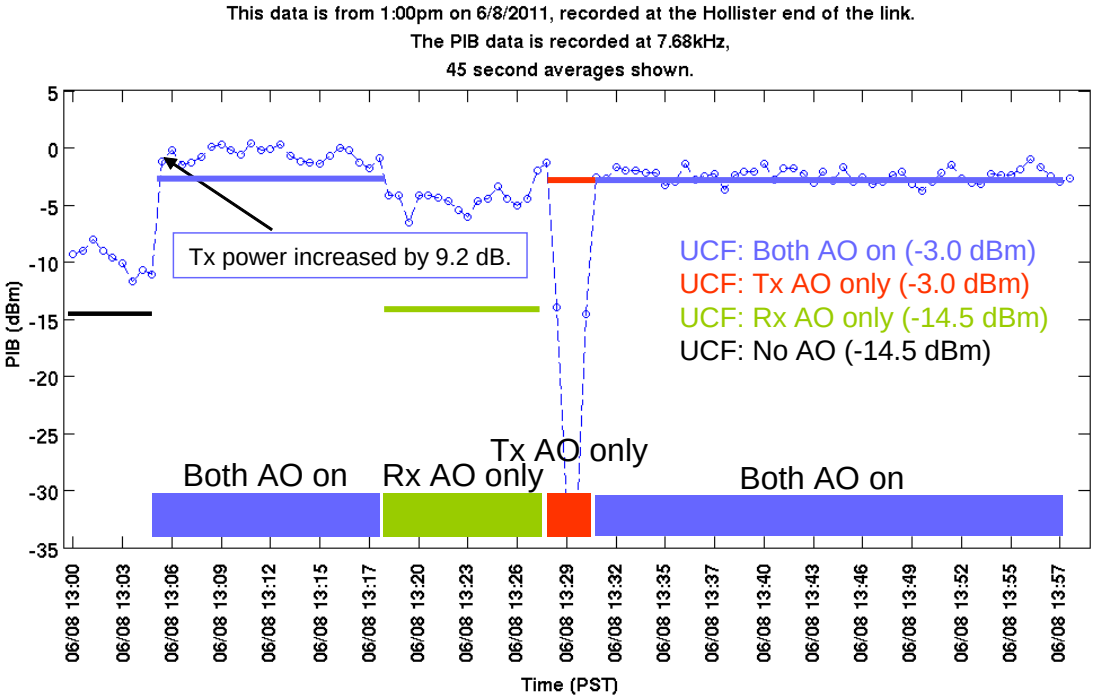

(b)

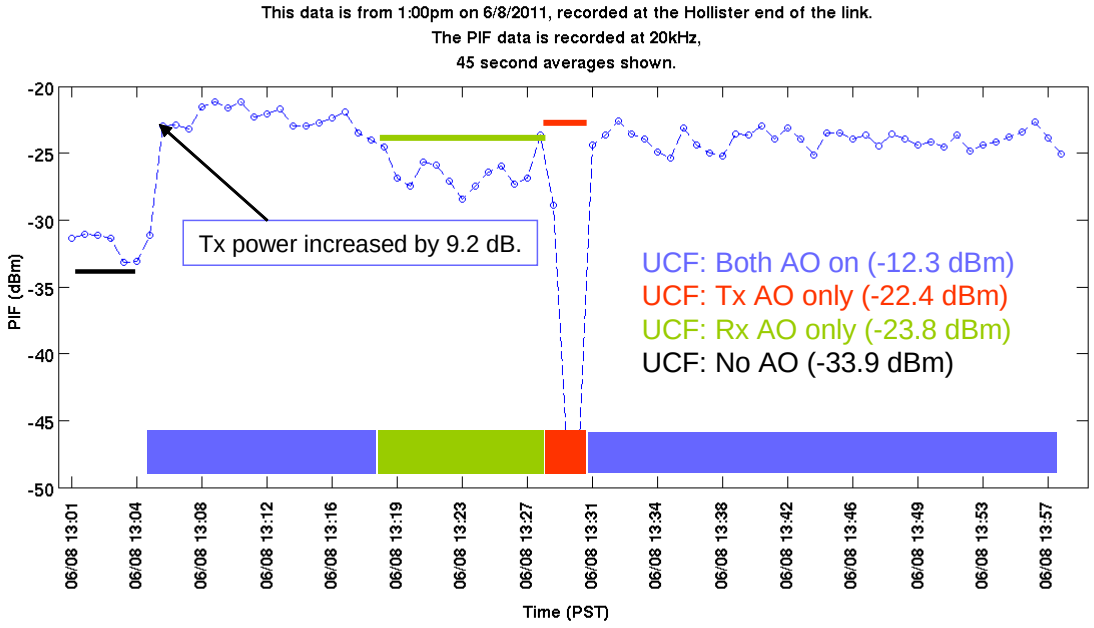

Figure 17 (*a*) PIB data taken during 1:00-2:00 pm on June 8 at the Hollister end of the path and (*b*) PIF data taken at the Hollister end of the path during the same time.

(a)

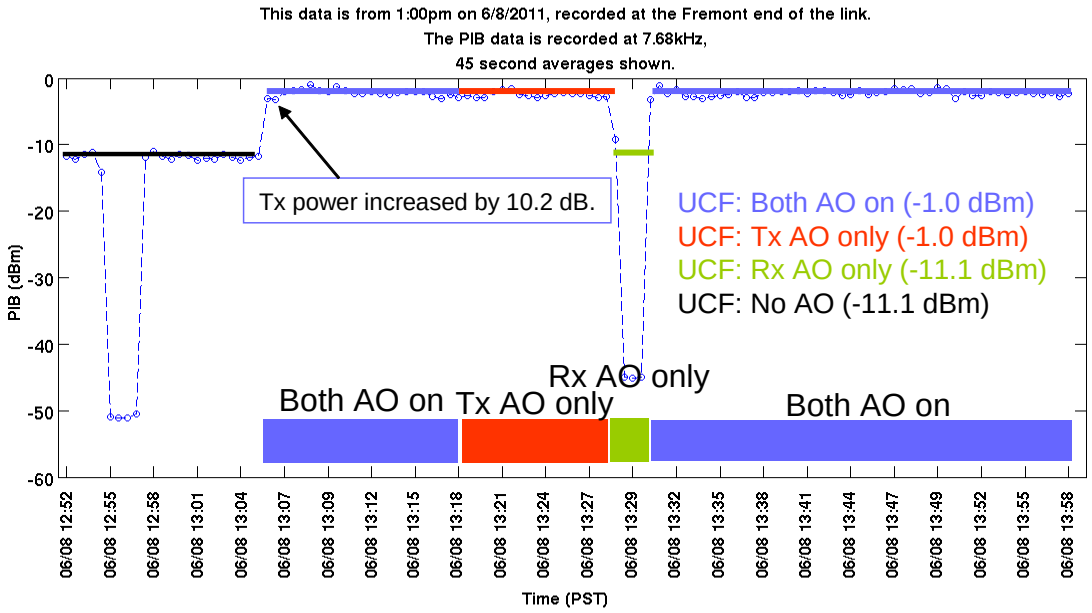

(b)

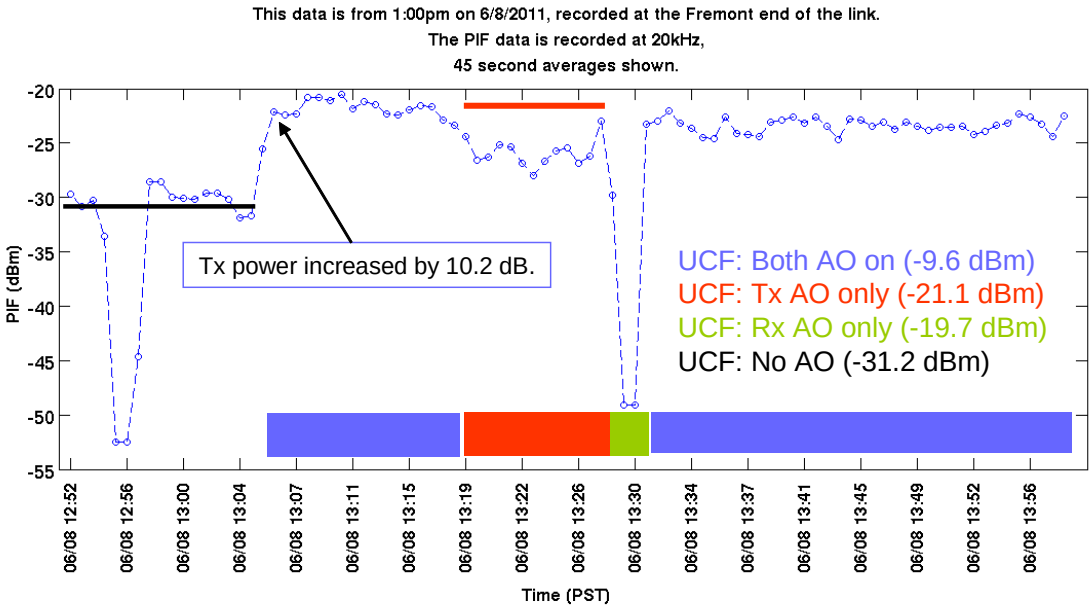

(*b*)

Figure 18 (*a*) PIB data taken during 1:00-2:00 pm on June 8 at the Fremont end of the path and (*b*) PIF data taken at the Fremont end of the path during the same time.

The reason for the discrepancy between PIF theory and measurements illustrated in Figs. 17 and 18 is not known for certain. However, it is possible that the AO theoretical model is not correct for calculating all Rx losses, although it did produce excellent results compared with measurements during one test period (Figs. 15 and 16). More likely, owing to large fluctuations in the PIF data caused by atmospheric turbulence and leading to mode mismatch between the received beam and that required by the fiber, it is possible that the Rx AO subsystem could not fully align the beam into the fiber during most of the runs.

6. DATA ANALYSIS AT CHINA LAKE

Further and final testing of the FOENEX system was conducted at the Naval Air Weapons Station in China Lake, California during March and April of 2012. When fully employed, there were three aircraft (Twin Otters) in the sky, each with two mounted skyballs. One skyball was mounted in the nose of the aircraft and the other on top of the aircraft. One of the three Twin Otter aircrafts used during the testing is shown in Fig. 19 with the two skyball locations clearly marked. In addition, there were two ground stations located on a peak site known as G6. The nominal range from the ground station to the aircraft was typically 50 km.

Figure 19 Twin Otter aircraft used for testing at China Lake.

The UCF team operated essentially the same as done earlier at Hollister Air Base. The Three-Aperture Scintillometer System (TASS) this time was mounted on a tracker on the G6 site at China Lake that was fed GPS coordinates of the aircraft location. At times when GPS was not available, manual tracking was employed. Manual tracking worked reasonably well owing to the slow movement of the aircraft in its triangular or figure eight patterns. The TASS system received the fluctuating beacon beam as before and used these results to estimate path-averaged values of the three atmospheric parameters.

6.1 UCF Experimental Setup at Site G6

The experimental setup and testing for UCF and APL took place at China Lake at an elevated site called G6. The purpose of the UCF testing was to characterize the Free-space Optical Experimental Network Experiment (FOENEX) channel conditions via measurements of turbulence parameters. The UCF TASS instrument consists of three telescopes with aperture sizes 7 cm, 12 cm, and 26.5 cm. Airplane beacon irradiance data were recorded in a continuous fashion as the TASS was kept within instrument field of view by UCF's GPS-automated tracking mount. The beacon operated at a wavelength of 780 nm. The tracking mount was also outfitted with three additional telescopes for fine tracking, two of which were wide field of view and the other a narrow field of view. Aircraft beacon video data were recorded at 30 frames per second by a Prosilica camera-telescope system co-aligned with and positioned adjacently to the TASS system. Channel conditions were compared with separate scintillometer and weather measurements taken atop the G6 site. A pre-test was performed prior to arriving at China Lake at the ISTEF Laser Test Range at Kennedy Space Center (KSC) to verify the test plan.

In Fig. 20 we show the UCF tracker mount with the TASS at G6, Fig. 21 shows the UCF field office at the site, and Fig. 22 features the UCF team.

Data recorded by UCF

The following characteristics were measured using the UCF TASS instrument:

- Airplane beacon irradiance data at 10 kHz rate.
- Refractive index structure parameter (C_n^2), inner scale of turbulence (l_0), and outer scale of turbulence (L_0)
- Airplane video data at a 30 fps rate.

The following atmospheric conditions were also measured at a height of 1-2 meters above the surface of the test range (same as the optical propagation path):

- Refractive index structure parameter (C_n^2) and inner scale of turbulence (l_0)
- Average wind velocity and direction (at 2.6 meters and 2 meters)
- Air temperature (at 2 meters, 1 meter, and ground level)
- Relative humidity

- Barometric pressure
- Solar irradiance

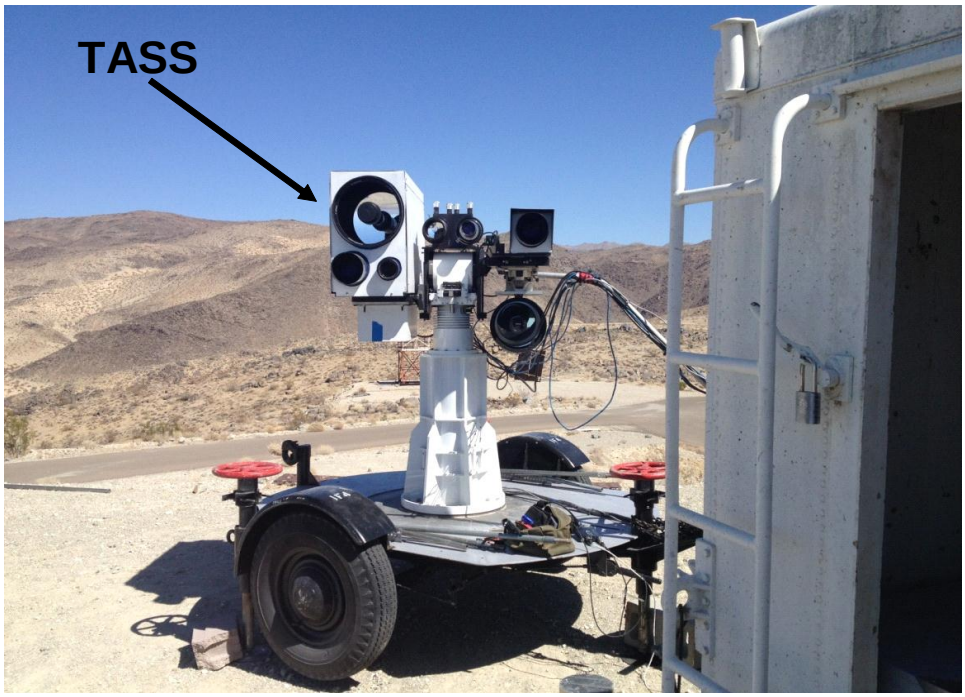

Figure 20 UCF tracker mount with Three-Aperture Scintillometer System (TASS).

Figure 21 UCF equipment and connex container (office).

Figure 22 UCF team at G6 site at China Lake.

6.2 UCF Data Collection

UCF Weather Station/ SLS-20 Scintillometer

UCF deployed its own weather station at G6 to capture ground level macro meteorological conditions. This data include temperature, wind velocity, barometric pressure, solar irradiance, and relative humidity. UCF also deployed a commercial Scintec SLS-20 scintillometer to simultaneously measure C_n^2 and inner scale l_0 near the ground at the data collection site. The data collected by the UCF TASS were correlated with measurements from the SLS-20 scintillometer as well as time of day, target/source height above ground level (AGL), and weather conditions from the weather station. A schematic of the weather and scintillometer equipment is shown in Fig. 23. Pictures of the actual setup at the G6 site are shown in Figs. 24 and 25.

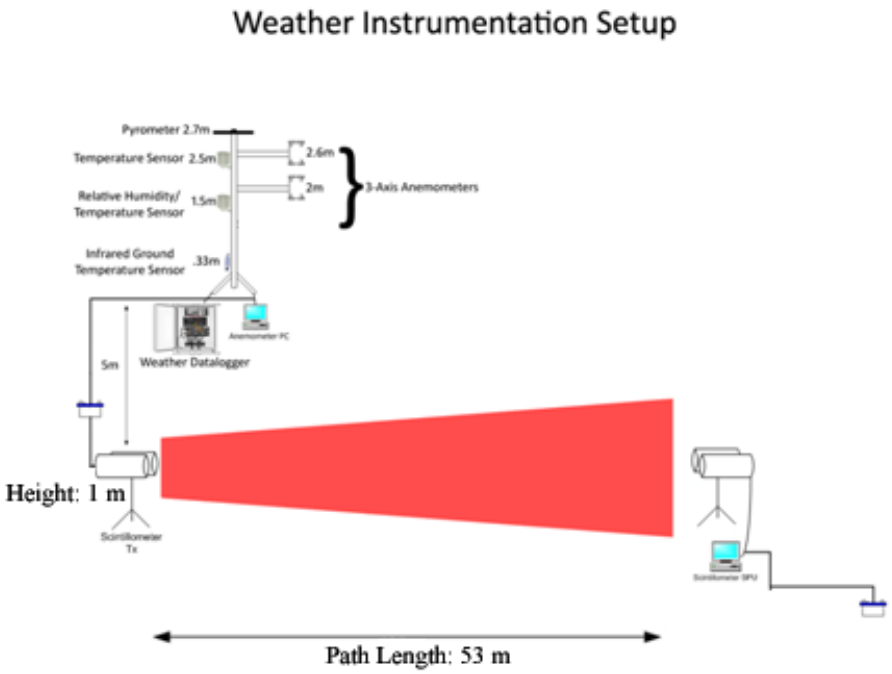

Figure 23 UCF weather station and SLS-20 schematical setup.

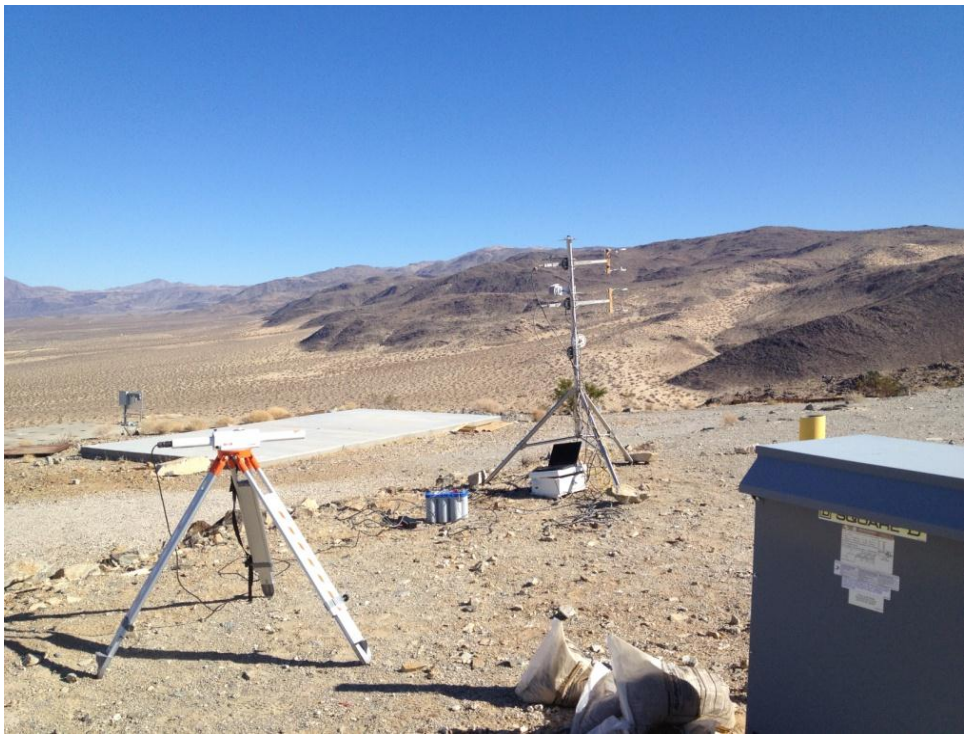

Figure 24 UCF weather station and SLS-20 transmitter.

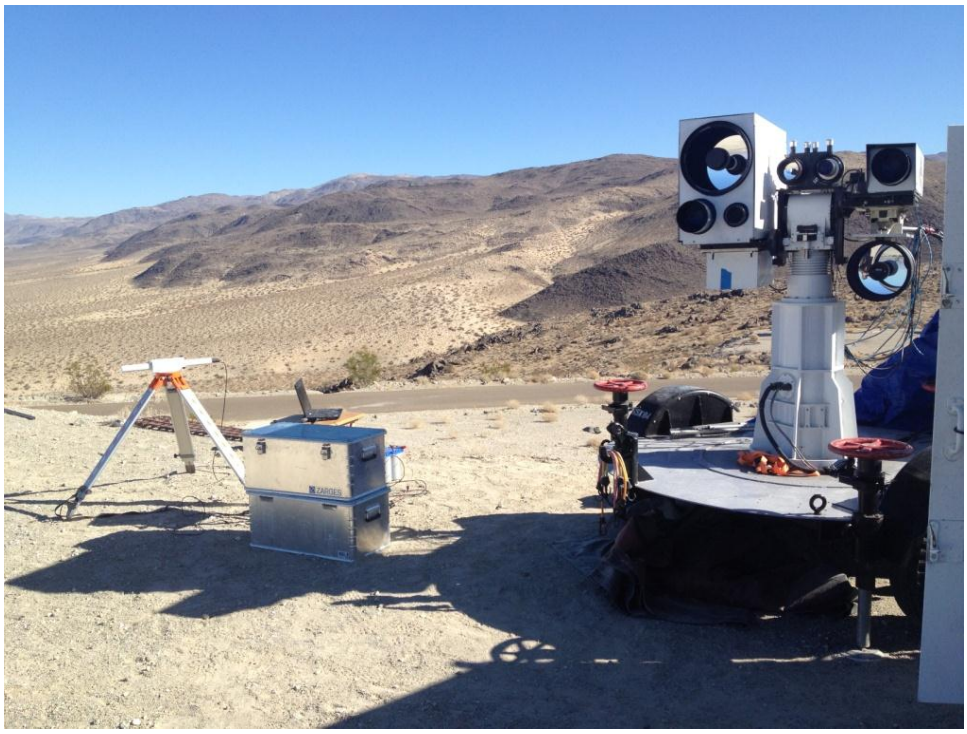

Figure 25 UCF TASS and SLS-20 receiver

TASS Data Collection

Avalanche photo diode voltage signal collected with LabView utilizing National Instruments 9234 24-Bit digitizer. Irradiance voltage signal was collected by digitizer within a ±5 volt input range. The digitizer recorded at 10k samples/sec.

TASS Video Data Collection

Prosilica camera recorded at 10 frames per second.

TASS Spare Aperture Video Data Collection

The following three figures demonstrate the TASS spare aperture video data of the Twin Otter aircraft's laser beacon (780 nm) at China Lake on Monday April 2, 2012. The telescope utilized a Prosilica camera that recorded at 30 frames per second.

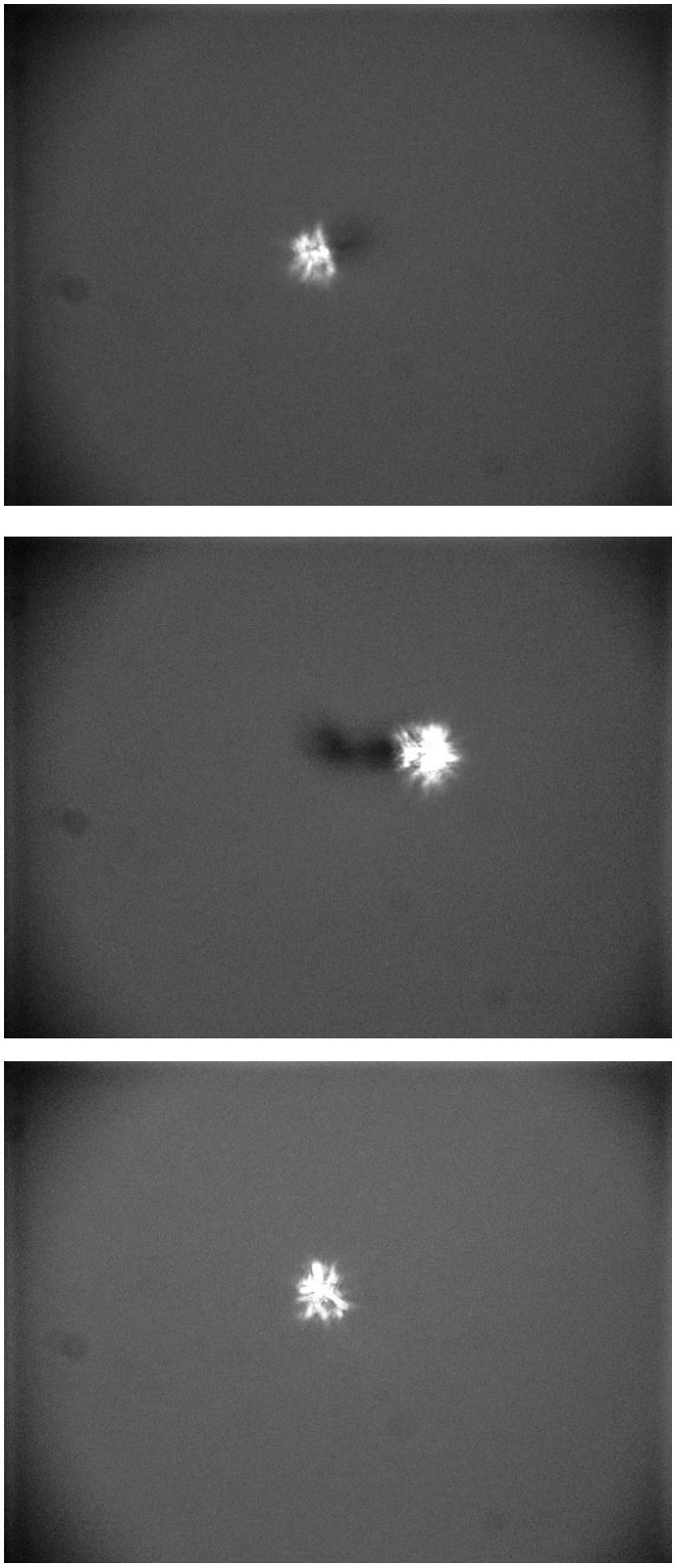

Figure 26 TASS spare aperture video data of the Twin Otter aircraft's laser beacon taken on April 2, 2012.

SLS-20 Data Collection

The Scintec SLS-20 scintillometer provides one minute averages of C_n^2 and inner scale l_0. Instruments were set up over a path length of 53 m and a height of 1 – 1.5 m.

GPS Data Collection

Received 1Hz updates of GPS data when beacon was "On" via ethernet port.

Weather Data Collection

Weather instruments were recording at 20 times/min and processed data were averaged over durations of one minute. Data collected includes temperature (ground level, 1.5 m, and 2.5 m), relative humidity at 1.5 m, and solar flux at 2.7 m. Plots of temperature, relative humidity, and solar flux data collected during the China Lake FOENEX experiments conducted on April 2 and April 3, 2012 are shown below in Figs. 27-29 and 30-32, respectively. Time is given in UTC and local time (PST) is defined by UTC – 8 hrs.

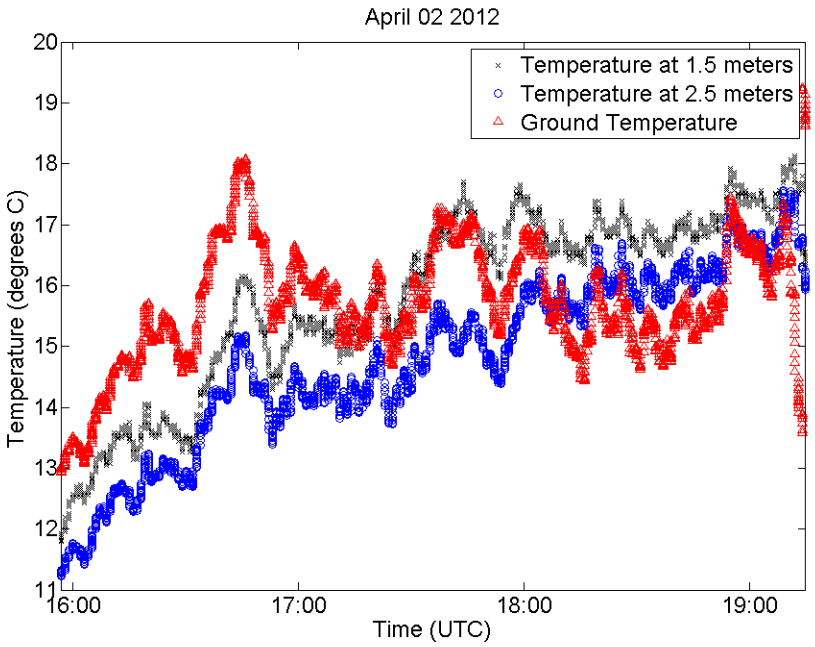

Figure 27 Temperature data April 2, 2012.

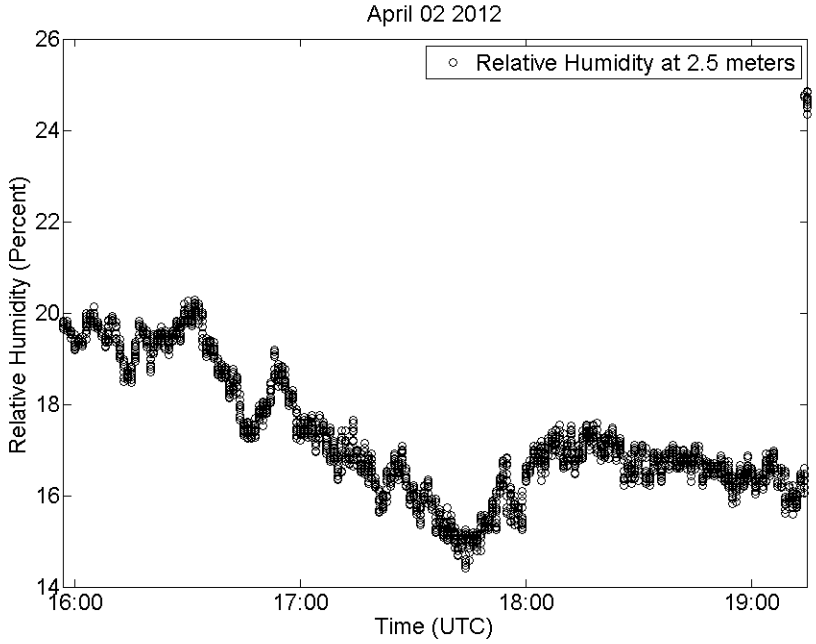

Figure 29 Relative humidity data April 2, 2012.

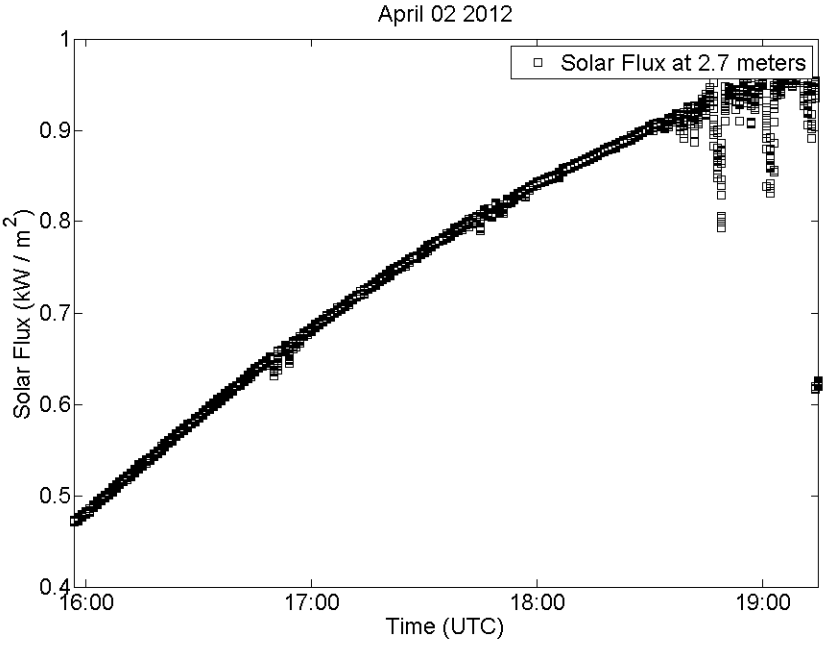

Figure 29 Solar flux data April 2, 2012.

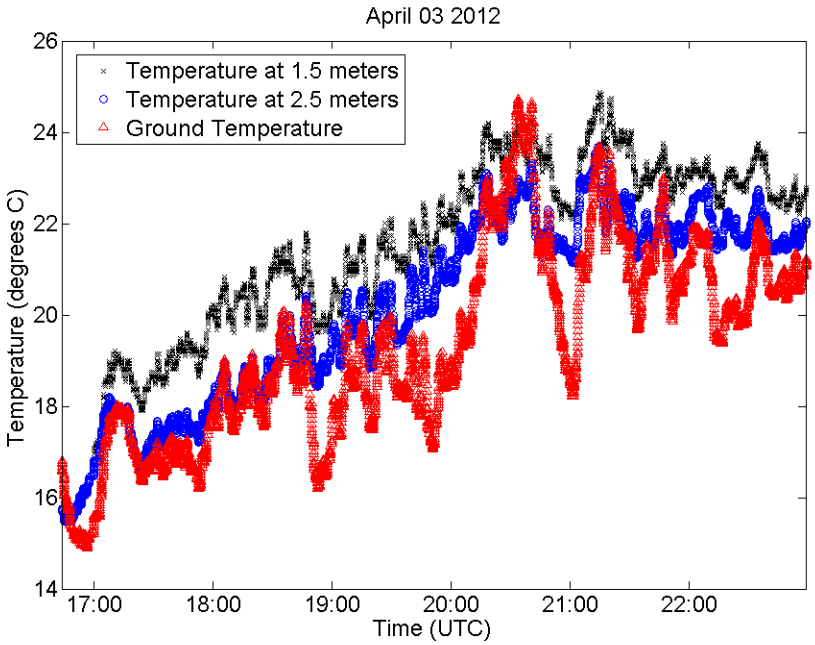

Figure 30 Temperature data April 3, 2012.

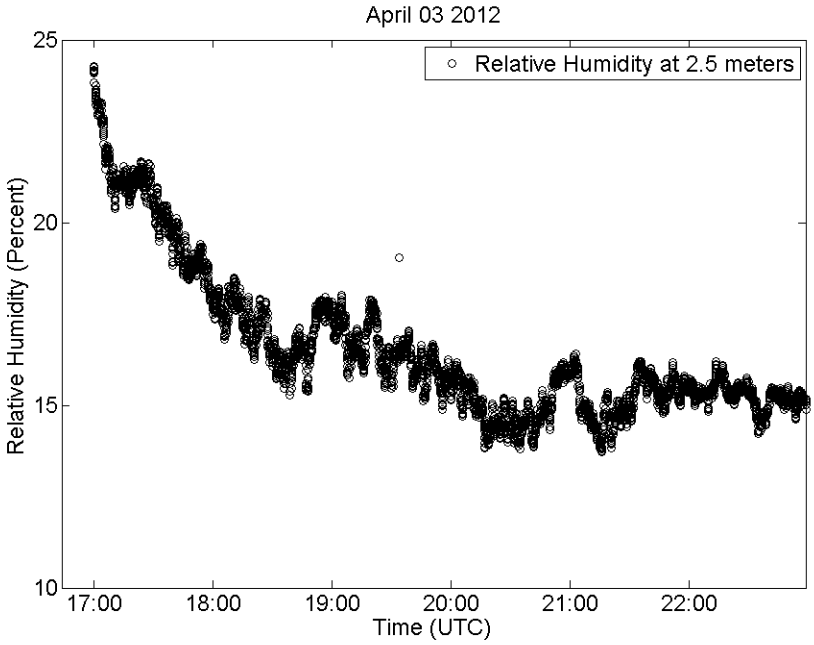

Figure 31 Relative humidity data April 3, 2012.

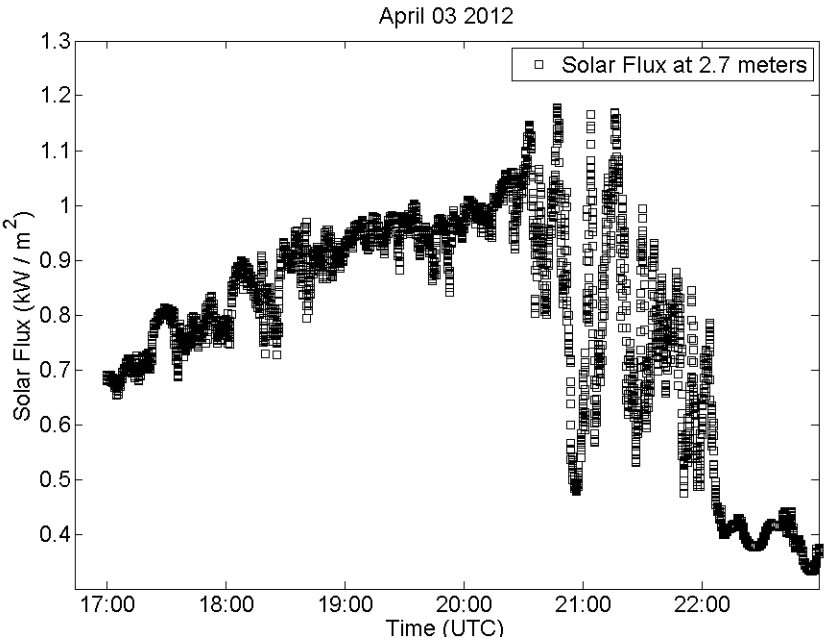

Figure 32 Solar flux data April 3, 2012.

Anemometer Data (Top and Middle Level) Collection

Anemometer data provided three-dimensional wind velocity at heights of 2 m and 2.6 m at a rate of 10Hz. Processed data were averaged over durations of twenty minutes. Mean value and standard deviation were computed for each data segment. Wind gust is calculated by adding three standard deviations to the mean value of wind speed. Data collected during FOENEX experiments at China Lake are shown below for April 2 and April 3, 2012.

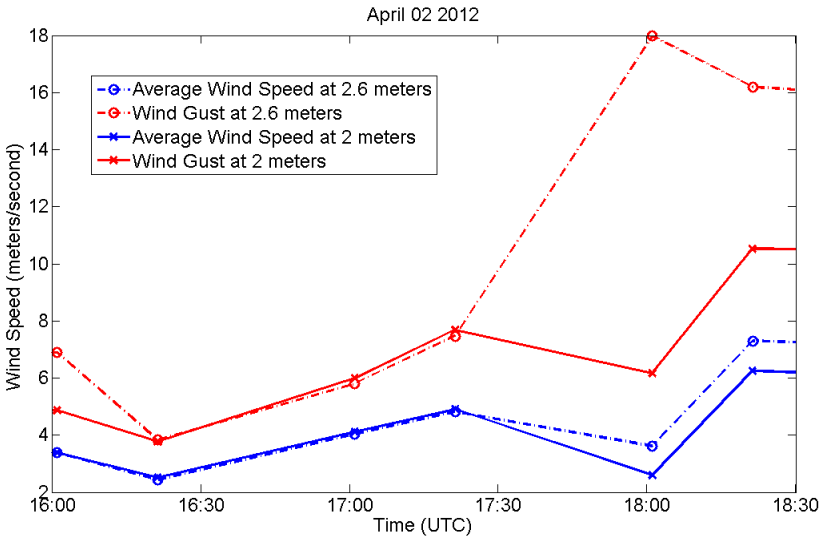

Figure 33 Wind data April 2, 2012.

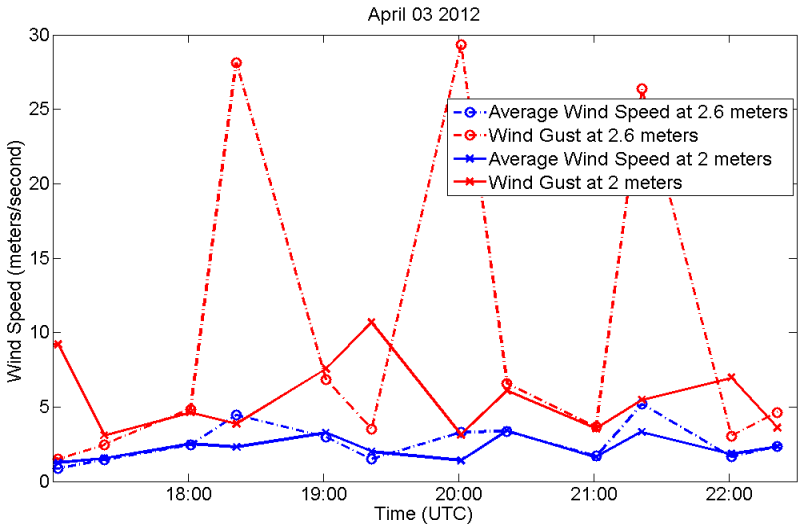

Figure 34 Wind data April 3, 2012.

6.3 TASS Path-Average C_n^2 Values: Theory

Prior to making measurements during the China Lake campaign, the UCF team did a theoretical analysis to estimate what conditions might be like during the actual testing at China Lake. This analysis included an air-to-ground path at 50 km range, ground-to-air path at 50 km range, and an air-to-air path at 100-km and 200-km ranges. In all cases we assumed a path-average C_n^2 value from air-to-ground of 1×10^{-16} $m^{-2/3}$, transmit power of 40 dBm (minus transmitter losses), and the aircraft altitude was taken at 4500 m.

In Figs. 35 and 36 we show power in the bucket (PIB) predictions for an air-to-ground path at 50 km range and a reciprocal ground-to-air path at 50 km range, both as a function of local time of day. Sunrise and sunset were set at 7:00 am and 7:00 pm, respectively. In the absence of adaptive optics (AO), we show the estimated PIB with and without the aero-optic effect from the aircraft in the downlink path in Fig. 35. In this analysis the aero-optic effect led to roughly a 2 dB loss in PIB that could be compensated for with the Tx AO subsystem turned on. For the uplink path in Fig. 36, there is no appreciable aero-optic effect from the aircraft. In Figs. 37 and 38 we show the estimated PIB values for an air-to-air path at ranges of 100 km and 200 km, respectively, also as a function of local time of day. In this case the aero-optic effect led to PIB reductions of 4 to 6 dB, depending on range.

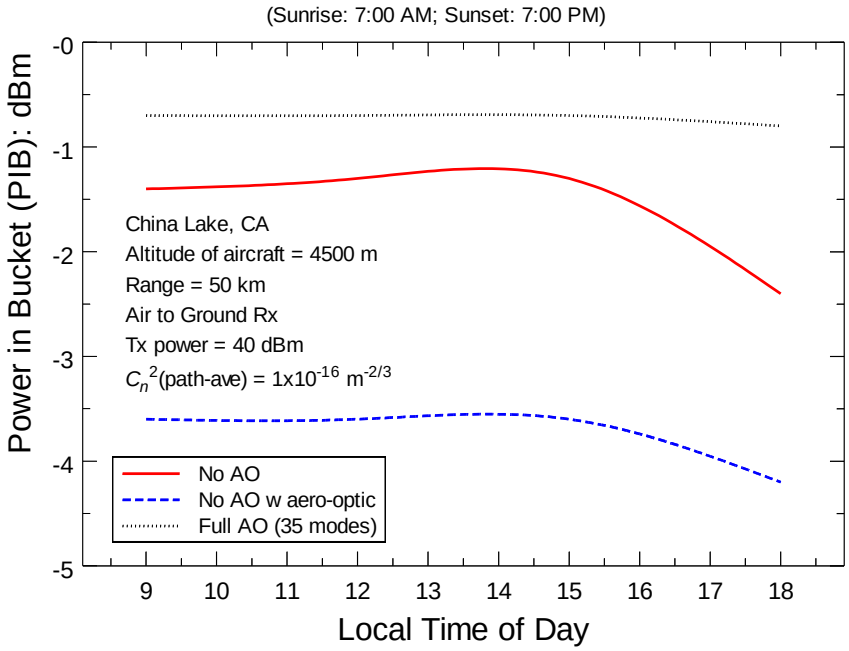

Figure 35 Theoretical estimation of PIB for a downlink path from the aircraft to ground as a function of local time of day.

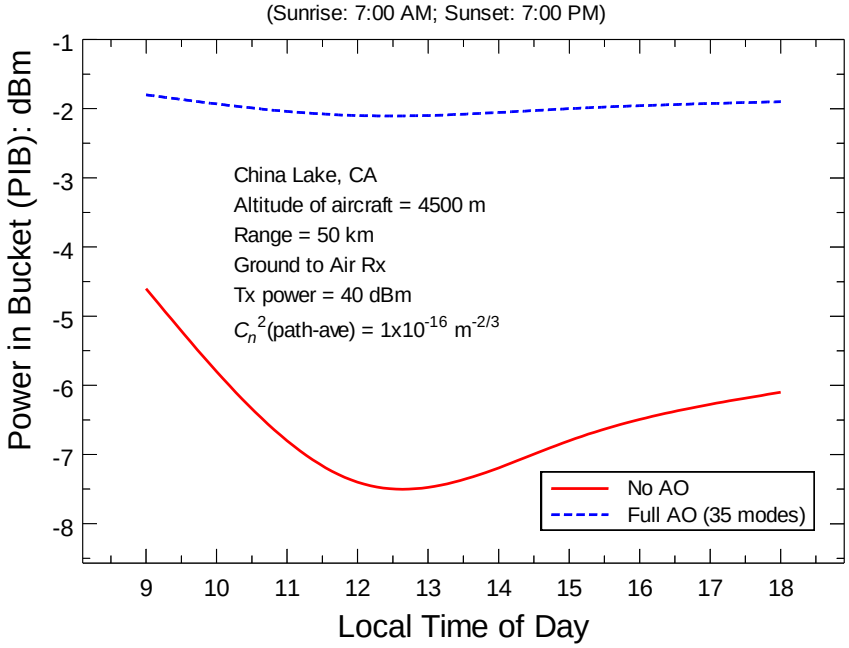

Figure 36 Same as Fig. 35 for an uplink path.

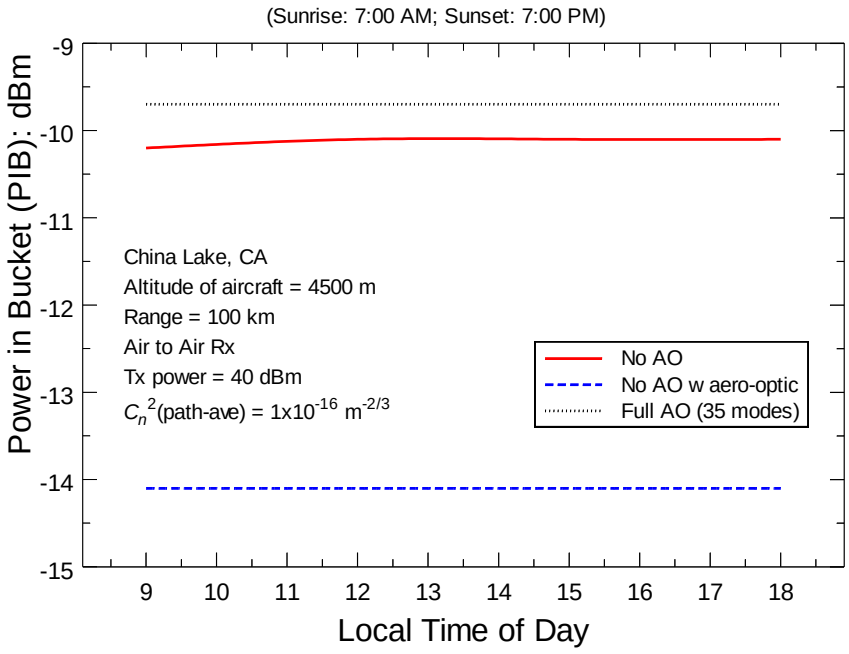

Figure 37 Theoretical estimation of PIB for an air-to-air 100-km path as a function of local time of day.

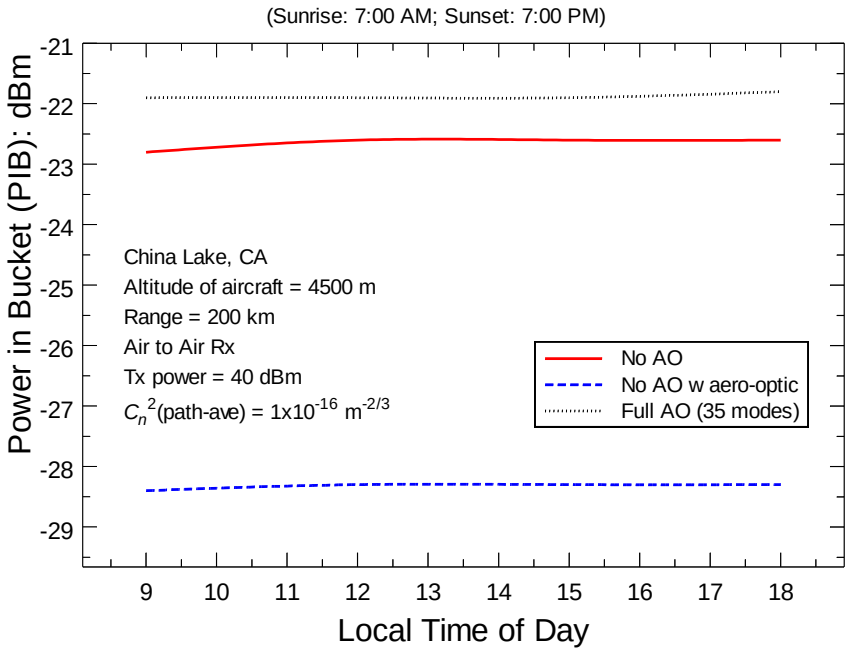

Figure 38 Same as Fig. 37 for a 200-km path.

6.4 TASS Path-Average C_n^2 Values: Measured

During March 19-21, 2012, the UCF team set up the SLS-20 scintillometer and other weather instrumentation to record atmospheric conditions. During this time period one aircraft was flying at roughly 3500 m altitude at a range of roughly 50 km (GPS data was not available to UCF so exact altitude and range were unknown). TASS data collected on March 20 is shown in Fig. 39 with 1-min averages. Here we also show 1-hr averages (dashed blue lines) between 11-12, 12-13, and 13-14 hours.

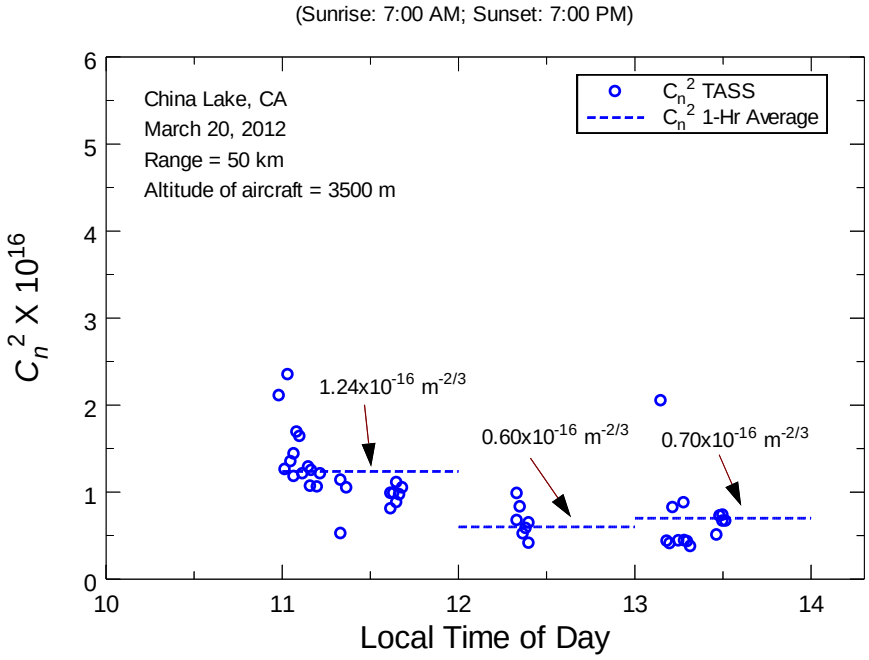

Figure 39 TASS path-average data collected on March 20, 2012.

TASS data were also collected on several days when all aircraft were flying and GPS data were available during the China Lake campaign. Because all aspects of the FOENEX system were working best on the days of April 2 and 3, 2012, we will present the TASS data and subsequent analysis for only those days. In Figs. 40 and 41 we have plotted the path-averaged values of C_n^2 calculated by TASS over 2-s intervals of averaging and over 45-s intervals of averaging. The data sets on April 2 show a fair amount of scatter as well as some of the data collected on April 3 between 13:43 and 14:13. The exception to this scatter is that in Fig. 41 for the early timeframe up to 13:43 local time and after 14:13. For these short periods of time the atmospheric conditions stayed fairly consistent. Times when a lot of scatter exists in the computed path-average parameters is most likely due to the changing conditions in the propagation path. Also the movement of the airborne platform creates turbulence just at the beacon beam's aperture, and this too will create changing conditions on the order of milliseconds.

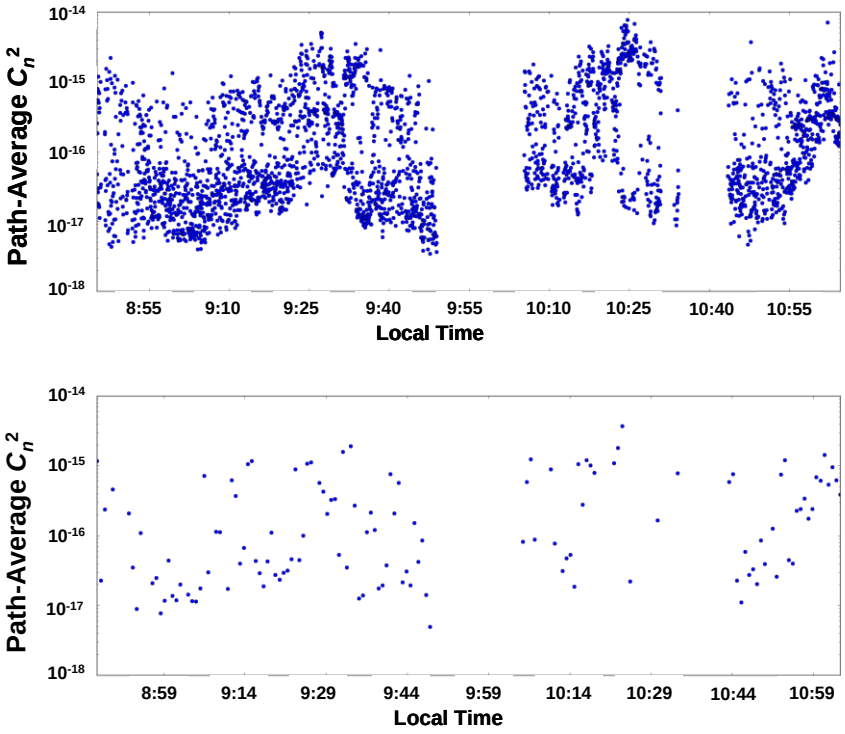

Figure 40 Path-average values of C_n^2 taken by TASS from aircraft to ground on April 2, 2012 at China Lake, CA. The unit on the vertical axis is $m^{-2/3}$. Upper figure is based on 2-s averages and the lower figure is based on 45-s averages.

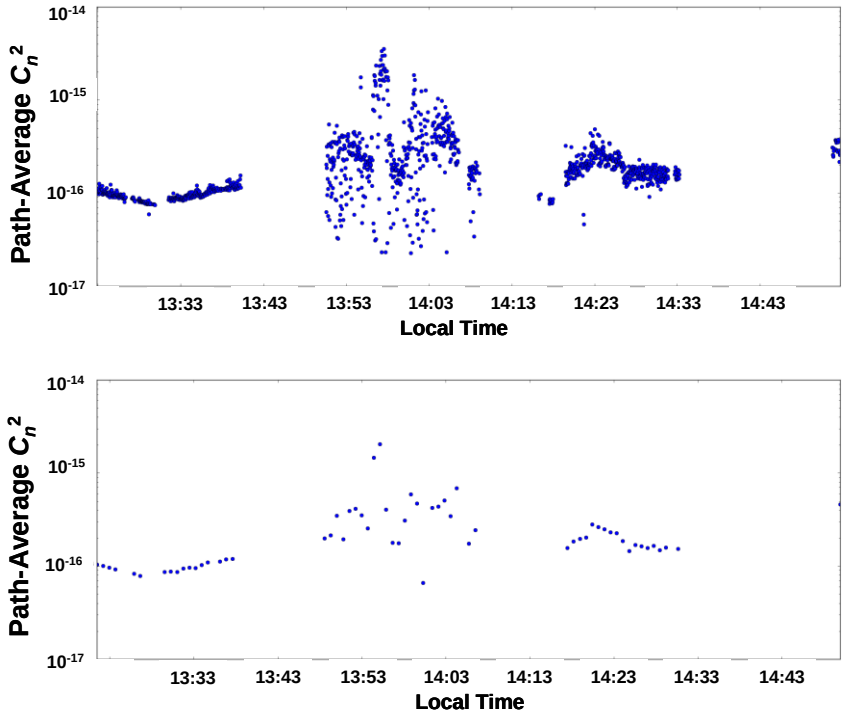

Figure 41 Same as Fig. 40 for April 3, 2012.

6.5 HAP Model Predictions for C_n^2, l_0 Near the Ground

Based on the path-average values given in Figs. 39-41, we use the HAP model to predict the C_n^2 values and inner scale l_0 values near the ground (at $h_0 \sim 1.0-1.5$ m). To do so, the model requires the range to the aircraft from the ground station, altitude of the aircraft above sea level, time of day, and path-average value of C_n^2 and l_0 along the path from the aircraft to the ground. The HAP model prediction for C_n^2 near ground level on March 20 is shown in Fig. 42 (open blue circles) along with SLS-20 Scintec scintillometer measurements (red triangles). The solid blue line in Fig. 42 is based on a 1-hr average between 13-14 hours and extrapolated to cover several other hours. Inner scale measurements from the SLS-20 scintillometer were not processed for this date.

On April 2 and 3 the aircraft altitude was nominally around 4500 m but at least one data point was obtained at altitude 2700 m. Range from the aircraft varied from 33 km to 73 km. Several representative values of near ground C_n^2 values based on the HAP model are shown in Figs. 43 and 44 for the days of April 2 and 3 (blue open circles). In addition, an average value of near ground C_n^2 as predicted by the HAP model is shown by the blue horizontal line in each figure. Also plotted are the measured values of C_n^2 at the same height above ground as measured by the SLS-20 Scintec scintillometer (red closed triangles).

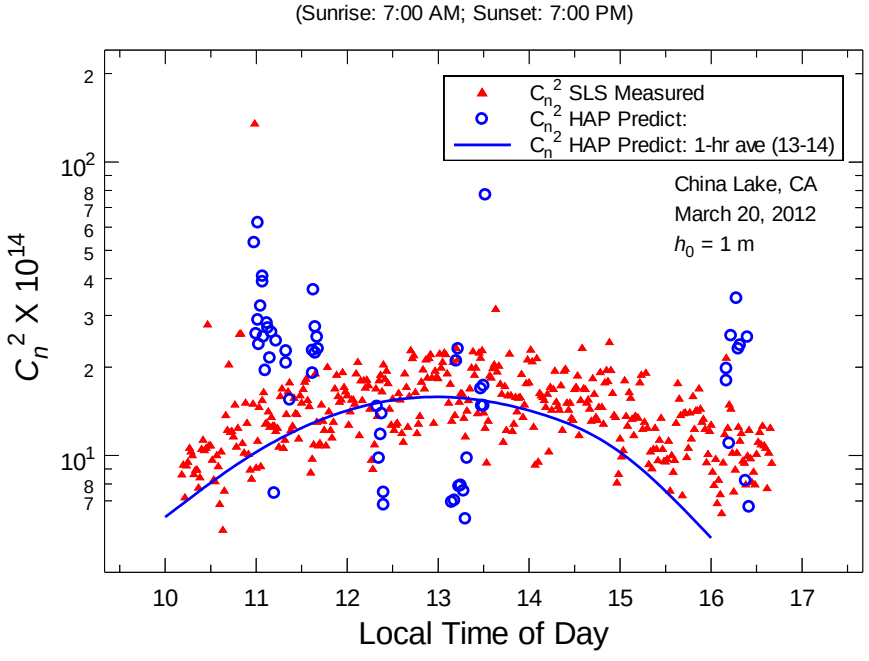

Figure 42 HAP model prediction based on TASS data in Fig. 39.

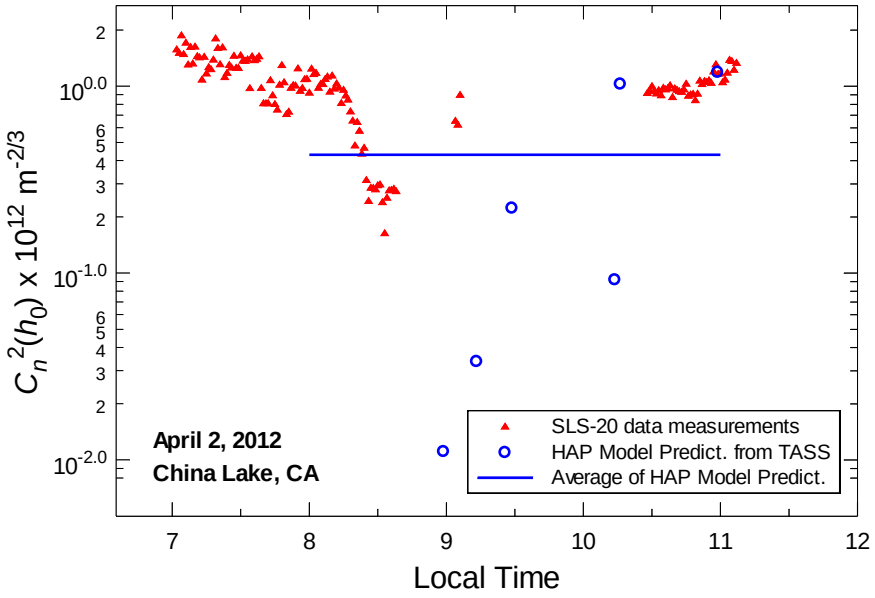

Figure 43 SLS-20 C_n^2 data (red triangles) measured near ground on April 2, 2012. Also shown are several values of near ground C_n^2 based on the HAP model prediction (blue circles) and an average value of near ground C_n^2 (blue line) extrapolated to extend between 8-11 hours local time.

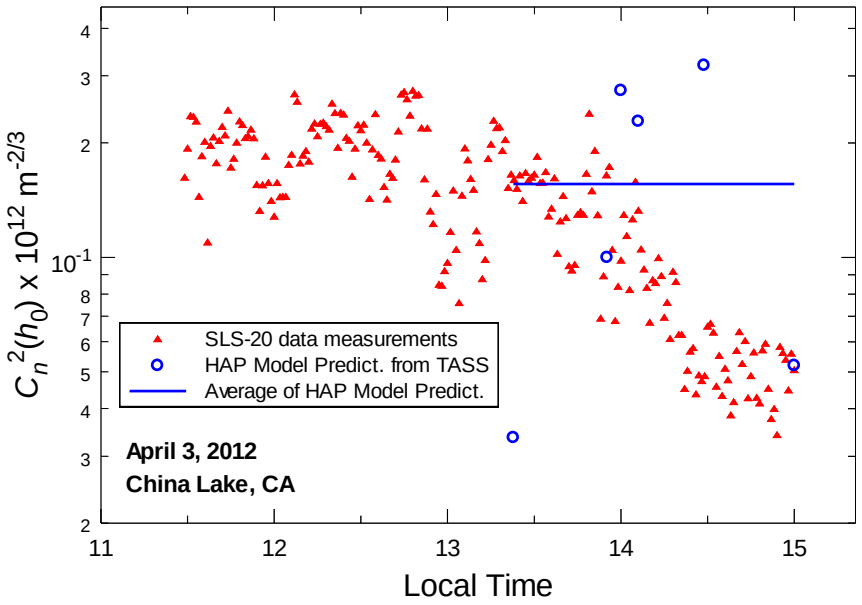

Figure 44 Same as Fig. 43 for April 3, 2012.

SLS-20 inner scale measurements near the ground for April 2 and 3, 2012 are shown in Figs. 45 and 46, respectively, by the filled red triangles. Because the TASS data on April 2 was widely scattered (e.g., see Fig. 40), the path-average inner scale values predicted by TASS were much too large to be realistic so it was impossible to predict inner scale values near the ground using the HAP model. On April 3, the data were considerably more consistent (see Fig. 41) and path-average inner scale values were estimated between 1 and 13 cm with an average value of 4.47 cm. By using this average value for the TASS data on April 2 (ignoring the unrealistically high values calculated by TASS on April 2), we obtained the solid blue curve in Fig. 45 for an estimation of near ground inner scale. The solid blue line in Fig. 46 is the estimated near ground inner scale value for April 3. On both days the estimated near ground average inner scale is consistent with that measured by the SLS-20 scintillometer.

Outer scale values near the ground are currently not measured by any instrument. Measured path-average values by TASS on April 2 generally varied from 1 to 4 m whereas those on April 3 were generally between 1 and 2 m. A rule of thumb for outer scale near the ground is on the order of the height of the point of interest, i.e., 1 m or less for China Lake setup.

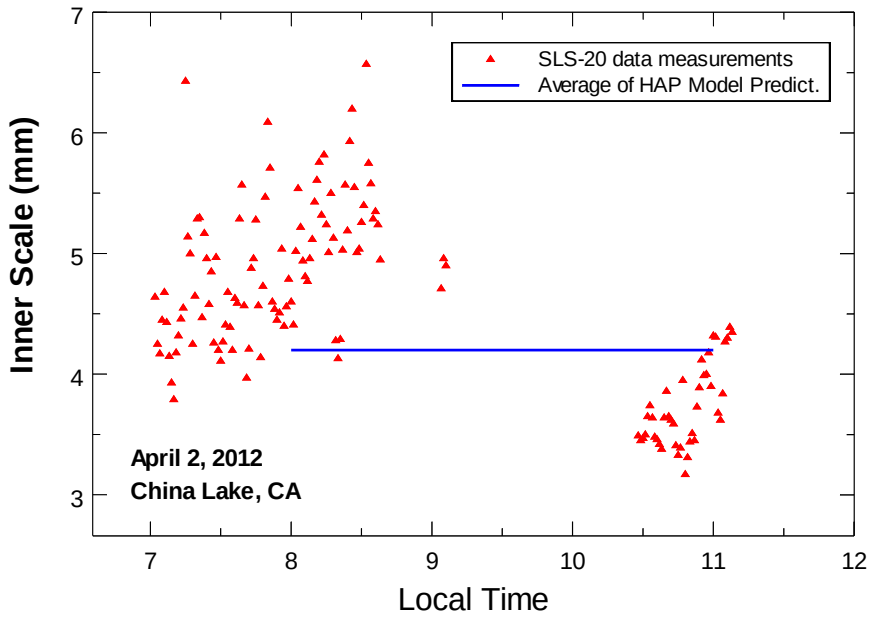

Figure 45 SLS-20 inner scale data (red triangles) measured near ground on April 2, 2012. Also shown is an average value of near ground inner scale (blue line) extrapolated from April 3 TASS data and HAP model to extend between 8-11 hours local time.

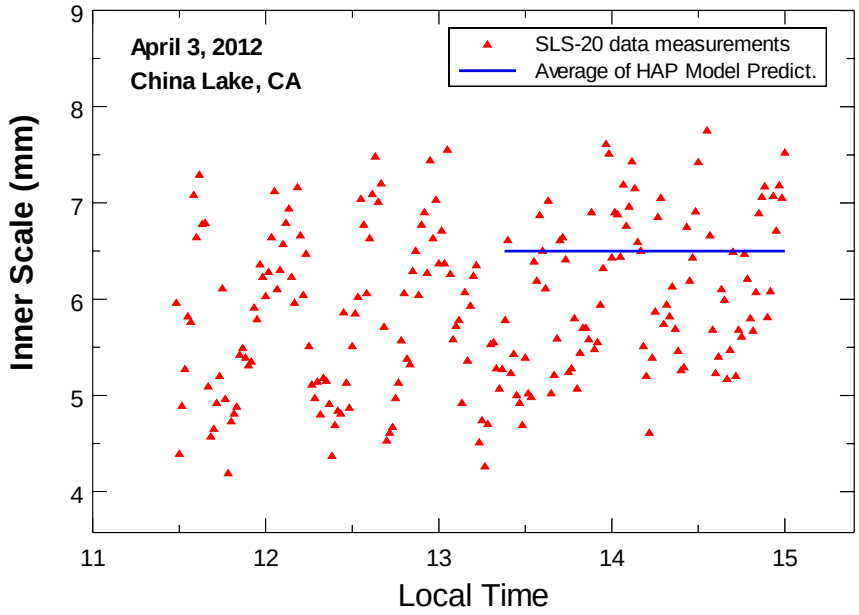

Figure 46 Same as Fig. 45 for April 3, 2012.

6.6 Fried Parameter from HAP Model

Next we provide estimates of the Fried parameter r_0 for a collimated Gaussian beam operating at 1550 nm over a 50-km path between an aircraft and ground. In Fig. 47 we illustrate how r_0 changes as a function of local time of day for three distinct values of path-average C_n^2. In Fig. 48 we show the reverse path from the ground to the aircraft at the same range. Clearly the statistics are not reciprocal between downlink and uplink. Last, in Fig. 49 we present estimates for the Fried parameter between two aircraft at the same altitude and ranges of 100 and 200 km.

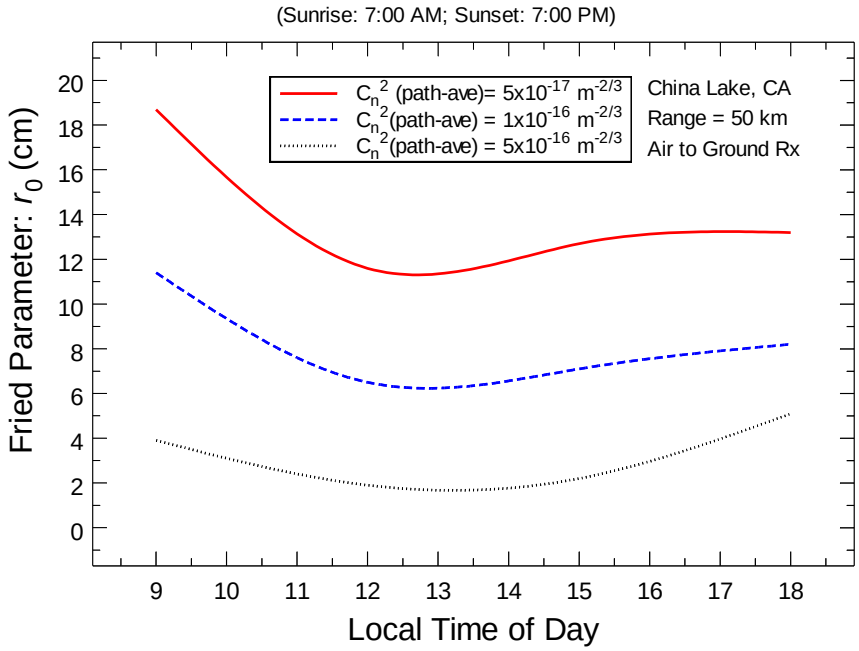

Figure 47 Theoretical estimate of r_0 as a function of local time of day for a downlink 50-km path from an aircraft to ground. The path-average C_n^2 values are assumed constant throughout the time shown.

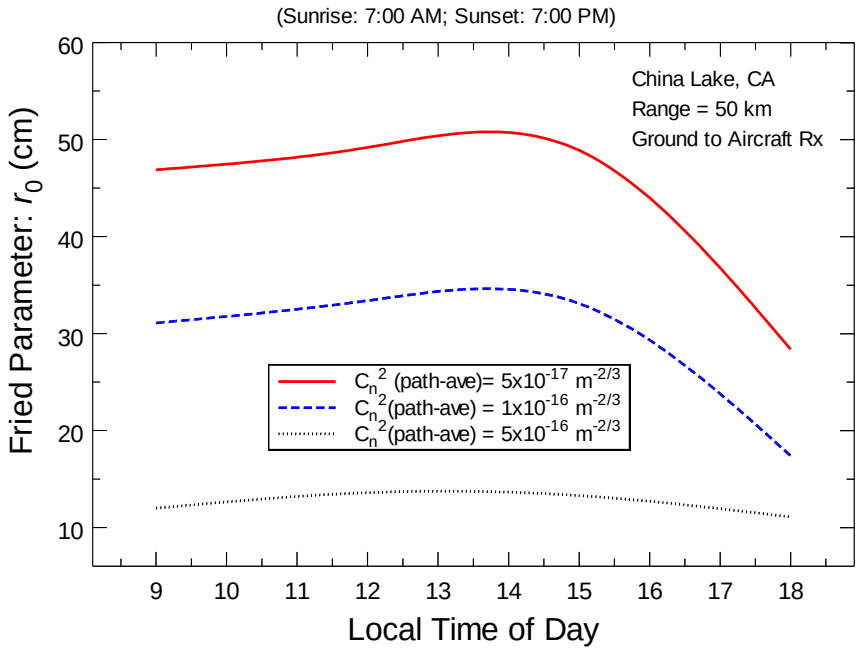

Figure 48 Theoretical estimate of r_0 as a function of local time of day for an uplink 50-km path from ground to an aircraft. The path-average C_n^2 values are assumed constant throughout the time shown.

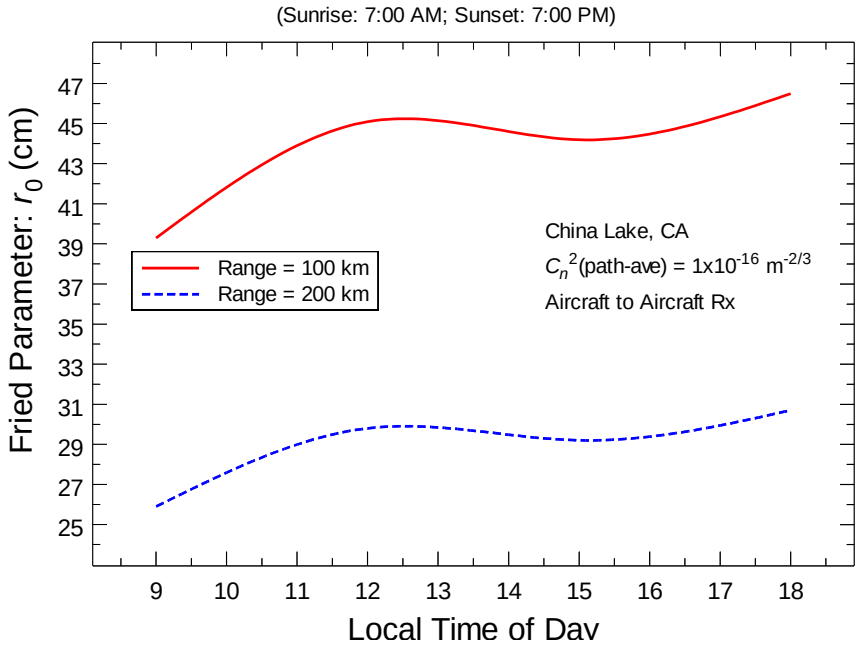

Figure 49 Theoretical estimate of r_0 as a function of local time of day for an optical link between two aircraft flying at the same altitude. The path-average C_n^2 value is assumed constant throughout the time shown.

6.7 Data Beam Analysis: PIB and PIF for Air to Ground Path

PIB Analysis

PIB and PIF data from APL was provided to and analyzed by the UCF team for the testing on April 2 and 3, 2012. In Fig. 50 we plot the April 2 measured PIB data (blue) for the downlink and uplink paths between ground and air in the upper two charts, the gimbal data during flight time in the next chart, and the measured TASS path-average C_n^2 data in the lower chart (same as that in Fig. 40). This data correspond to several ranges from aircraft to ground with an average range of approximately 47 km. By taking the average of the TASS C_n^2 data during this period we calculated a path-average value of $C_n^2 = 2.23\times10^{-16}$ m$^{-2/3}$ (solid blue curve in lowest chart). The average UTC time was roughly 17:50 hrs, the uplink Fried parameter was 21.3 cm, the downlink Fried parameter was 4.9 cm, and the combination of these average values led to a theoretical average value for PIB with full AO that was 0.0 dBm (downlink) and -1.7 dBm (uplink) shown by the horizontal blue lines in the upper two charts of Fig. 50. Clearly, these average theoretical PIB estimates are quite reasonable compared with actual measured PIB data. In the UCF analysis it was assumed that the boundary layer aero-optic effect on the downlink beam was mostly corrected by the Tx AO subsystem. The uplink beam is not affected by this boundary layer around the aircraft. Finally, the parameters in the HAP model used for this theoretical analysis are: $M = 2.33$, $p = 1.25$, and $C_n^2(h_0) = 3.15\times10^{-13}$ m$^{-2/3}$.

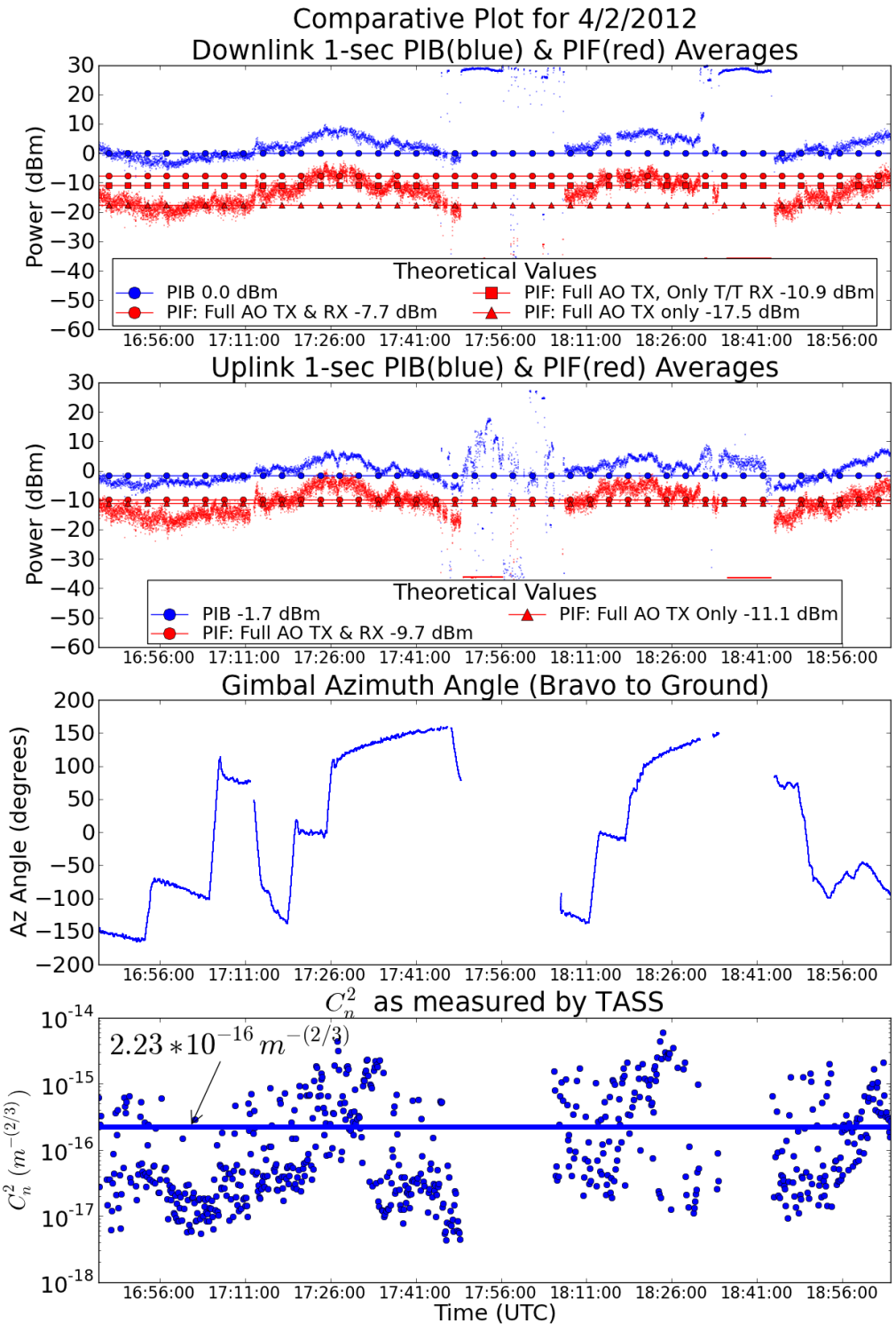

Figure 50 Measured values of downlink/uplink PIB data (blue in upper two charts) and PIF data (red in upper two charts) between ground and aircraft taken on April 2, 2012 at China Lake, CA. The blue lines represent theoretical estimates based on a full AO system. The red lines are based on full Tx AO and Rx AO (top), or only tip-tilt at the Rx (middle), or no Rx AO (bottom). The third chart from the top gives the gimbal angle at the aircraft and the lowest chart represents TASS data (same as Fig. 40) obtained during the same time period. The solid blue line is the TASS data average value.

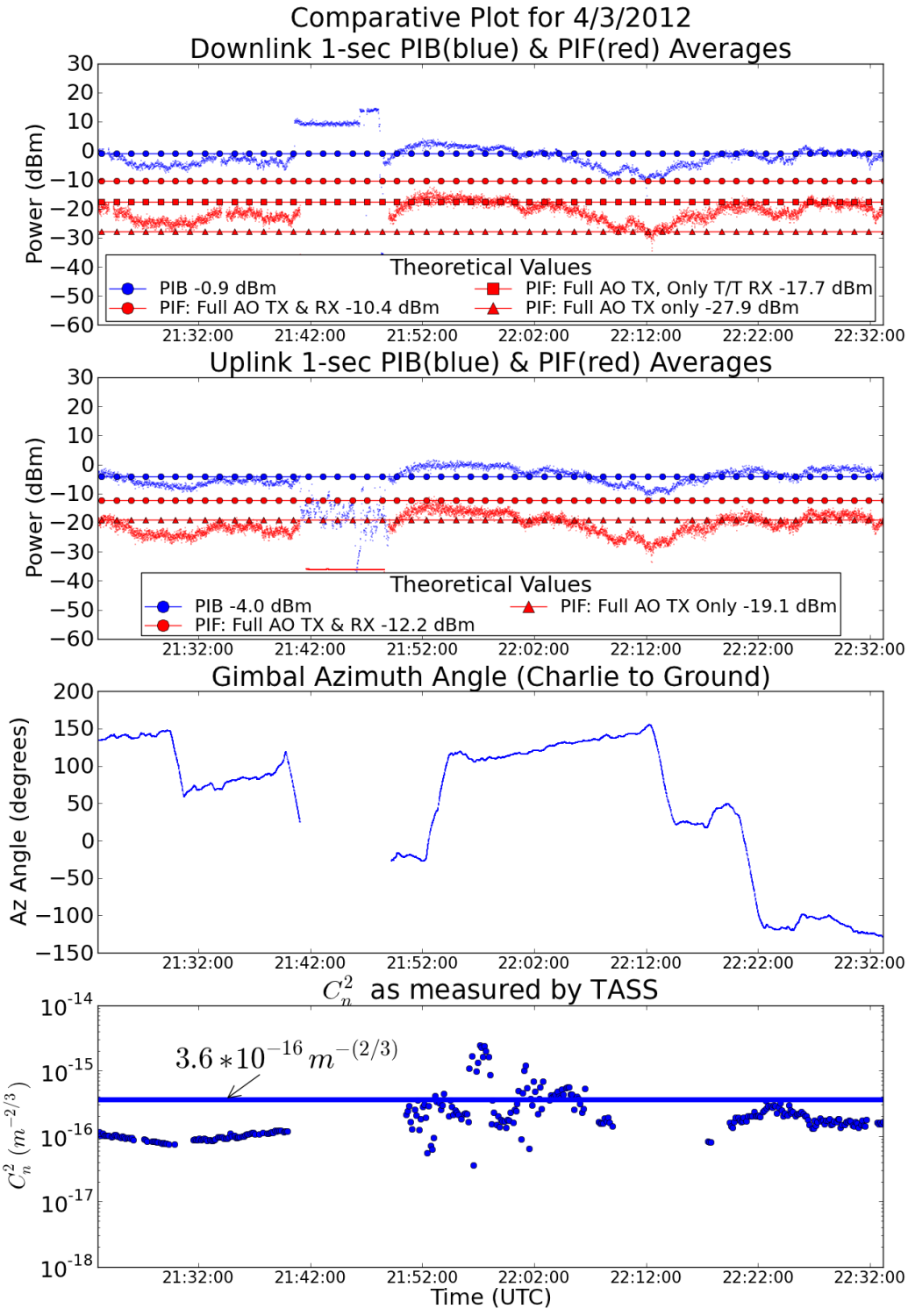

Figure 51 Same as Fig. 50 for April 3, 2012. TASS data same as that in Fig. 41.

In Fig. 51 we show the same analysis for April 3 as provided in Fig. 50 for April 2. Here the downlink average theoretical estimate is –0.9 dBm and the uplink estimate is –4.0 dBm. On this date, the TASS path-average value was $C_n^2 = 3.6\times10^{-16}$ m$^{-2/3}$, the uplink Fried parameter was 16.3 cm, and the downlink Fried parameter was 2.4 cm. The average UTC time was roughly 22:00 hrs. This data correspond to several ranges from aircraft to ground with an average range of approximately 50.6 km. Once again the average theoretical PIB estimates with full AO (solid blue lines) are consistent with measured PIB values. The parameters in the HAP model used for this theoretical analysis are: $M = 3.48$, $p = 1.43$, and $C_n^2(h_0) = 1.56\times10^{-12}$ m$^{-2/3}$.

PIF Analysis

Based on the above average results for C_n^2 and Fried parameter, the theoretical estimate for downlink PIF with full Tx and Rx AO on April 2 is –7.7 dBm (upper red line), leading to a PIF to PIB ratio of –7.7 dB with full AO subsystem working. Clearly, the theoretical result is a little high compared with the actual data. The theoretical result based on full Tx AO and Rx tip-tilt (T/T) is –10.9 dBm and that based on full Tx AO only (i.e., no Rx AO) is –17.5 dBm. Both of these latter theoretical results match the average measured data reasonably well. In this case the measured data lies roughly along the middle line, suggesting that atmospheric conditions were sufficiently bad that the higher-order AO corrections (beyond tip-tilt) were not always able to get the mode-mismatched light into the single-mode fiber. Possible reasons for the discrepancy between theoretical and measured PIF results are discussed in the next section on Concluding Remarks. On the uplink path the theoretical PIF estimate with full AO is –9.7 dBm with PIF to PIB ratio of –8.1 dB. For the uplink beam, all theoretical results are similar and match the measured PIF results reasonably well.

On April 3, the theoretical estimate for downlink PIF with full AO is –10.4 dBm (upper red line). For the downlink beam the PIF to PIB ratio is –9.4 dB. This theoretical result with full AO on lies above all the measured data. In fact, the downlink measured PIF lies between the theoretical result based on Tx AO and Rx T/T at –17.7 dBm and that based on Tx AO only at –27.9 dBm. Atmospheric turbulence conditions were stronger on April 3 than on April 2, and this probably accounts for much of the difference between theoretical and measured results. That is, atmospheric conditions were often too strong for the Rx AO system to provide full compensation. For the uplink beam the theoretical PIF with full AO is –12.2 dBm and the PIF to PIB ratio is –8.1 dB. For the uplink beam, the theoretical result with full Rx AO does not match the data well owing to the stronger turbulence conditions but that with Tx AO only provides a reasonable match with much of the measured PIF results.

6.8 Data Beam Analysis: PIB and PIF for Air to Air Path

PIB Analysis

The PIB and PIF data on April 2 between two aircraft is sparse and not very conclusive. Hence, we only present the data from April 3 during the same time frame as that for air-to-ground. In Fig. 52 we show the PIB and PIF data as well as average theoretical curves based on the HAP model used for Fig. 51 and ranges of 40 and 160 km. The theoretical results at 40 km and 160 km are based on a full Tx and Rx AO system. Also, the assumed atmospheric attenuation loss varies between 2.4 (40 km) and 9.7 dB (160 km), depending on range.

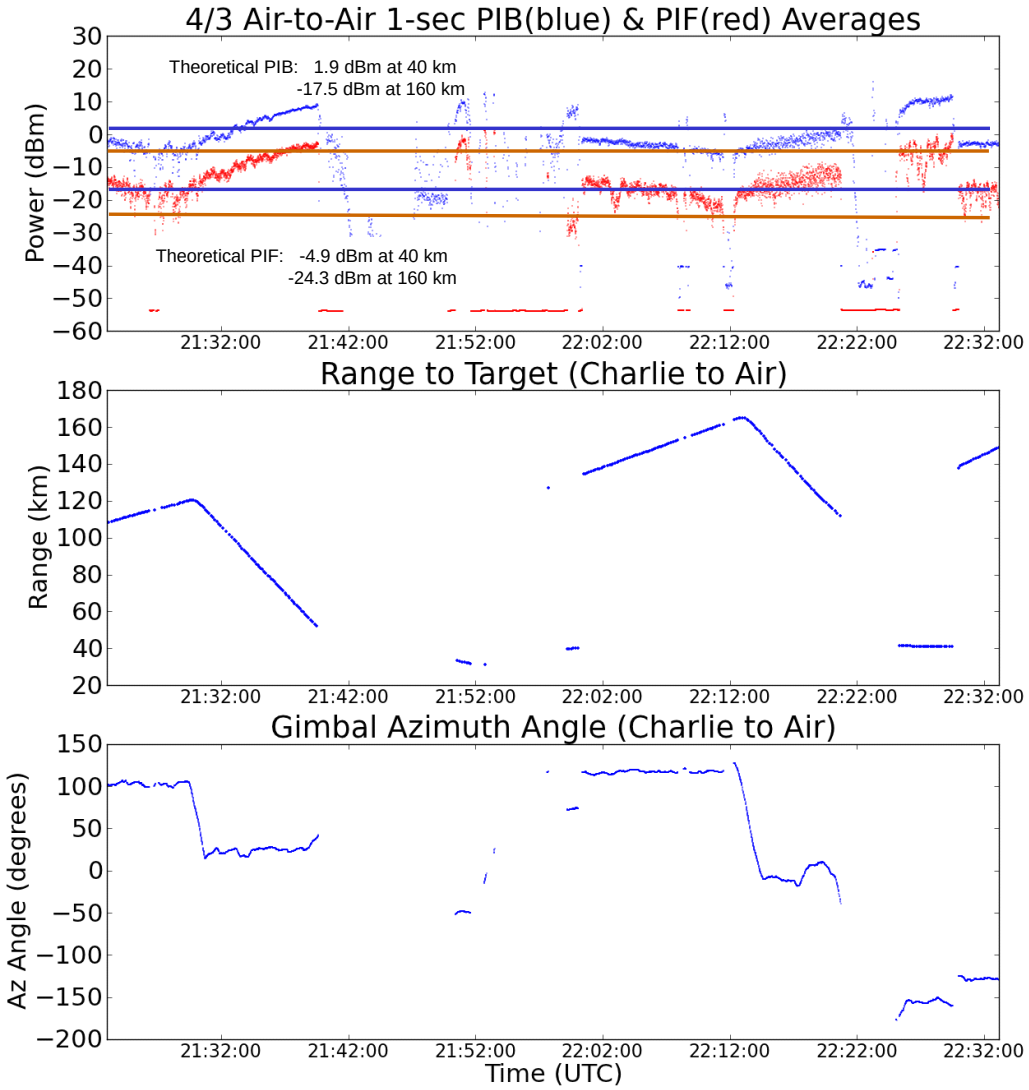

Figure 52 Measured values of air-to-air PIB data (blue in upper chart) and PIF data (red in upper chart) between two aircraft taken on April 3, 2012 at China Lake, CA. The solid blue and red lines represent theoretical estimates at the extreme ranges based on a full AO system. The third chart gives the gimbal angle at the aircraft.

7.0 CONCLUDING REMARKS

In this Final Report we have presented results of the UCF atmospheric path-average measurements taken at Hollister Air Force Range in California during June 2011 and at the Naval Air Weapons Test Range in China Lake, CA during March-April 2012. The purpose of these measurements was to ascertain the atmospheric channel conditions during testing of the FOENEX hybrid communication system. In addition, UCF used the path-average data to construct a C_n^2 profile model, called the HAP model, that was subsequently used to perform a theoretical analysis of the data link PIB and PIF between ground and aircraft at various ranges from 30 km out to approximately 75 km, and between two aircraft at ranges out to 160 km. This theoretical analysis is useful in validating the theoretical model and then determining how well the communication system worked during the actual testing at these test sites. In particular, one can determine the effectiveness of the AO subsystem under these same atmospheric conditions. Validating the theoretical model also permits analysis of other scenarios (air-to-ground, air-to-air, etc.) at other places around the globe given that the atmospheric channel is reasonably well known.

In order to construct useful theoretical models for predicting system performance under a wide variety of atmospheric conditions it is important to have a good understanding of the particular channel of interest. For instance, when treating propagation between a ground terminal and a flying airborne terminal, it should be recognized that the effects of turbulence on the uplink and downlink optical waves are usually not reciprocal. This is so because the atmospheric turbulence is not distributed uniformly throughout the path. In addition, the airborne terminal can have a fairly strong turbulence layer generated very near the terminal due to the flight of the airborne platform. This optical turbulence near the airborne terminal is a very "thin sheet" called aero-optic boundary layer turbulence. This boundary layer turbulence is confined to a short distance (possibly only a few centimeters) compared with long slant paths to a ground terminal. In addition, the turbulence near the ground is usually strong but diminishes with altitude. Hence, with long slant paths, the propagation may extend through much of the strongest optical turbulence near the ground. The optical turbulence in the propagation path between the aircraft boundary layer and the ground is extremely weak by comparison.

When an optical wave passes through optical turbulence, the spatial wave-front is distorted. As the wave propagates further along the path these distortions begin to cause self-interference, leading to amplitude fluctuations over the cross-sectional profile of the beam wave. The spatial size of these local amplitude fluctuations is known as $r_{0.}$ Within these coherent patches the spatial phase is very "smooth," not varying more than one radian and with constant field amplitude within the patch. As a beam wave propagates continuously through optical turbulence, these r_0 patches get progressively smaller, reaching a small size determined by the physical spatial fluctuation of the turbulence of the air. There can be several of these small coherent patches in the receiver aperture and the field captured in the aperture would have both spatial phase and amplitude fluctuations. This is the case for a downlink optical wave from an airborne platform. On

the other hand, as an uplink beam wave propagates beyond turbulence into free space or into very weak turbulence approaching the airborne platform, these coherent r_0 patches expand due to beam wave diffraction. For the large coherent patches the receiver aperture would have both a smooth spatial phase over the receiver aperture and constant amplitude, but the captured field would appear to be "blinking" as the wind carries the various r_0 patches across the receiver aperture.

The adaptive optic (AO) system in FOENEX measures the spatial phase distortion across the wave-front entering the collecting aperture. The deformable mirror (DM) impresses a conjugate phase and focuses the incoming signal into the single mode fiber. If the incoming wave has amplitude fluctuations as well as phase, the AO cannot correct for that so as to match the necessary amplitude for coupling into the fiber. That is, if the amplitude of the incoming wave does not match that of the fiber's propagation mode, the coupling into the fiber will be low. On the other hand, the out-going wave from the fiber has the conjugate wave-front and compensates for the effect of that turbulence just in front of the collecting aperture (aero-optic boundary layer). Generally speaking, it's only the turbulence within the Rayleigh Range that can be compensated.

The propagation uplink/downlink paths at China Lake were very similar to that described above. The turret on the airborne platform was mostly perpendicular to the line of flight (see gimbal angle charts in Figs. 50 and 51) and this created optical turbulence immediately near the collection aperture. The ground terminal was located on a hill that was high with very steep slopes dropping off to the valley. The stronger turbulence was located close to the ground terminal. The extended path between the two terminals was always close to 50 km and the aircraft flew at altitudes above 12,000 ft (4500 m). Consequently, the r_0 coherent patches at the ground terminal were generally smaller than the receiver aperture (10 cm) whereas those at the airborne platform were always larger than the receiver aperture.

Our theoretical analysis of PIB data for both test sites (Hollister and China Lake) was fairly consistent with most of the actual measured data (see Figs. 15-18 and Figs. 50-52). In particular, it is believed that any beam wander or boundary layer aero-optic effect around the aircraft was always compensated for by the transmitter AO subsystem. Unfortunately, the good comparison between theoretical and measured PIB data did not always occur with the PIF data (shown in the same figures). That is, assuming the full Rx AO subsystem was effective, the theoretical estimate of average PIF was sometimes much higher than that of the measured data. In this case it was discovered that assuming the Tx AO subsystem correction was applied to the outgoing beam and either Rx T/T compensation or no Rx AO compensation was applied to the received beam, the theoretical PIF results were generally more consistent with the measured PIF data. Thus, it is believed that the receiver AO compensation system at Hollister and at China Lake was not always fully effective under the given atmospheric conditions.

8. REFERENCES

[1] F. Strömqvist Vetelino, B. Clare, K. Corbett, C. Young, K. Grant, and L. Andrews, "Characterizing the propagation path in moderate to strong optical turbulence," *Appl. Opt*. **45,** 3534–3543 (2006).

[2] D. T. Wayne, R. L. Phillips, L. C. Andrews, F. S. Vetelino, B Griffis, M. R. Borbath, D. J. Galus, C. Visone, "Measuring optical turbulence parameters with a three-aperture receiver," *Proc. SPIE* **6709** (2007).

[3] L. C. Andrews, R. L. Phillips, D. Wayne, T. Leclerc, P. Sauer, R. Crabbs, and J. Kiriazes, "Near-ground vertical profile of refractive-index fluctuations," *Proc. SPIE* **7324** (2009).

[4] L. C. Andrews, R. L. Phillips, R. Crabbs, D. Wayne, T. Leclerc, and P. Sauer, "Atmospheric channel characterization for ORCA testing at NTTR," *Proc. SPIE* **7588** (2010).

[5] L. C. Andrews and R. L. Phillips, *Laser Beam Propagation through Random Media*, 2nd ed. (SPIE Optical Engineering Press, 2005).

[6] R. R. Beland, "Propagation through atmospheric optical turbulence," in *The Infrared and ElectroOptical Systems Handbook*, F. G. Smith, ed. (SPIE Opt. Eng. Press, Bellingham, 1993), Vol 2, Chap. 2.

[7] C. E. Coulman, J. Vernin, Y. Coqueugniot, and J. L. Caccia, "Outer scale of turbulence appropriate to modeling refractive-index structure profiles," *Appl Opt.* **27**, 155-160 (1988).

[8] L.B. Stotts, J. Foshee, B. Stadler, D. Young, P. Cherry, W. McIntire, M. Northcott, P. Kolodzy, L. Andrews, R. Phillips, and Alan Pike; "Hybrid Optical RF Communications," Proceedings of the IEEE, Vol. 97, No. 6, pp 1109-1127, June 2009.

[9] D. Young, J. Sluz, J. Juarez, M. Airola, R. Sova, H. Hurt, M. Northcott, J. Phillips, A. McClaren, D. Driver, D. Abelson, J. Foshee, "Demonstration of high data rate wavelength division multiplexed transmission over a 150km free space optical link," Proc. SPIE 6578, Defense Transformation and Net-Centric Systems (2007).

[10] M. Northcott, A. McClaren, B. Graves, J. Phillips, D. Driver, D. Abelson, D. Young, J. Sluz, J. Juarez, M. Airola, R. Sova, H. Hurt, J. Foshee, "Long distance laser communications demonstration," Proc. SPIE 6578, Defense Transformation and Net-Centric Systems (2007).

[11] D. Young, J. Sluz, J. Juarez, M. Airola, R. Sova, H. Hurt, M. Northcott, J. Phillips, A. McClaren, D. Driver, D. Abelson, J. Foshee, "Demonstration of high data rate

wavelength division multiplexed transmission over a 150km free space optical link", MILCOM 2007, Advanced Communications Technologies 4.2, Directional Hybrid Optical/RF Networks (2007).

[12] J. Latham, M. Northcott, B. Graves, J. Rozzi, "IRON-T2 2008 AOptix Technologies Test Report," Contract FA8750-08-C-0185 (2009).